JNeurosci
THE JOURNAL OF NEUROSCIENCE

Research Articles: Development/Plasticity/Repair

Slow waves promote sleep-dependent plasticity and functional recovery after stroke

https://doi.org/10.1523/JNEUROSCI.0373-20.2020

Cite as: J. Neurosci 2020; 10.1523/JNEUROSCI.0373-20.2020

Received: 10 February 2020
Revised: 15 September 2020
Accepted: 24 September 2020

TITLE PAGE

Title: Slow waves promote sleep-dependent plasticity and functional recovery after stroke

Running title: Slow waves promote functional stroke recovery

Authors and affiliations: Laura Facchin[1], Cornelia Schöne[1], Armand Mensen[2], Mojtaba Bandarabadi[1], Federica Pilotto[1, 3], Smita Saxena[1, 3], Paul Antoine Libourel[4], Claudio L.A. Bassetti[1, 2#], Antoine R. Adamantidis[1, 2, 3 #*]

[1]Centre for Experimental Neurology, Department of Neurology, Inselspital University Hospital, University of Bern, 3010 Bern, Switzerland.
[2] Department of Neurology, Inselspital University Hospital, University of Bern, 3010 Bern, Switzerland.
[3] Department of Biomedical Research, University of Bern, 3010 Bern, Switzerland.
[4] Centre de Recherche en Neurosciences de Lyon, University of Lyon, 69500 Bron, France.

[#] equal contributions.
* correspondence should be addressed to:

Antoine Adamantidis, Department of Neurology, Inselspital University Hospital, University of Bern, Freiburgstrasse 18, 3010 Bern, Switzerland. e-mail: antoine.adamantidis.unibe.ch.

Claudio L.A. Bassetti, Department of Neurology, Inselspital University Hospital, University of Bern, Freiburgstrasse 18, 3010 Bern, Switzerland. e-mail: claudio.bassetti@insel.ch.

Number of pages: 45
Number of figures: 8
Number of words for:
abstract: 250
introduction: 493
discussion: 1474

Conflict of interest: The authors declare no competing financial interest.

Acknowledgment: We thank all members of the Adamantidis and Bassetti Labs and the technical assistance of Andrea Oberli and Joel Gyger. LF was supported by the Inselspital University Hospital of Bern and the SNF Sinergia (CRSII3_160803) grant. AA was supported by the Human Frontier Science Program (RGY0076/2012), Inselspital University Hospital of Bern, Swiss National Science Foundation (31003A_156156), European Research Council (725850), Sinergia (CRSII3_160803), the University of Bern and the Bern University Hospital.

Authors contribution: LF, FP, SS, CB and AA designed the research; LF and CS performed the research; LF, CS, AM, MB analyzed the data; PAL developed the sleep scoring system. All authors wrote the paper.

ABSTRACT

Functional recovery after stroke is associated with a remapping of neural circuits. This reorganization is often associated with low frequency high amplitude oscillations in the peri-infarct zone in both rodents and humans. These oscillations are reminiscent of sleep slow waves (SW) and suggestive of a role for sleep in brain plasticity that occur during stroke recovery, however, direct evidence is missing. Using a stroke model in male mice, we showed that stroke was followed by a transient increase in NREM sleep accompanied by reduced amplitude and slope of ipsilateral NREM sleep SW. We next used 5 ms optical activation of Channelrhodopsin 2-expressing pyramidal neurons, or 200 ms silencing of Archeorhodopsin T-expressing pyramidal neurons, to generate local cortical UP, or DOWN, states, respectively, both sharing similarities with spontaneous NREM SW in freely-moving mice. Importantly, we found that single optogenetically-evoked SW (SW^{opto}) in the peri-infarct zone, randomly distributed during sleep, significantly improved fine motor movements of the limb corresponding to the sensorimotor stroke lesion site, as compared to spontaneous recovery and control conditions, while motor strength remained unchanged. In contrast, SW^{opto} during wakefulness had no effect. Furthermore, chronic SW^{opto} during sleep were associated with local axonal sprouting as revealed by the increase of anatomical pre- and post-synaptic markers in the peri-infarct zone and corresponding contra-lesional areas to cortical circuit reorganization during stroke recovery. These results support a role for sleep SW in cortical circuit plasticity and sensorimotor recovery after stroke and provide a clinically-relevant framework for rehabilitation strategies using neuromodulation during sleep.

SIGNIFICANCE STATEMENT

Brain stroke is one of the leading causes of death and major disabilities in elderly worldwide. A better understanding of the pathophysiological mechanisms underlying spontaneous brain plasticity after stroke, together with an optimization of rehabilitative strategies, are essential to improve stroke treatments. Here, we investigate the role of optogenetically-induced sleep slow waves in an animal model of ischemic stroke and identify sleep as a window for post-stroke intervention that promotes neuroplasticity and facilitates sensorimotor recovery.

INTRODUCTION

Stroke is an acute brain injury caused by a sudden decrease in cerebral blood flow, followed by local inflammation (Huang et al., 2006), excitotoxicity (Lai et al., 2014) and cell death (Small et al., 1999). Changes in neuronal excitability after stroke are thought to promote long-term plasticity in surviving neurons that contributes to the reorganization of cortical maps and to the underlying level of axonal sprouting supporting brain functions (Carmichael, 2012; van Meer et al., 2012; Silasi and Murphy, 2014), as observed in rodents (Nudo, 1997; Murphy and Corbett, 2009; Carmichael et al., 2017) and humans (Khedr et al., 2005; Lindenberg et al., 2010). To date, pharmacological treatments and non-invasive brain neuromodulation techniques hold promise in improving plasticity and functional recovery both in animal model (Zhang et al., 2007; Yoon et al., 2012) and human (Robinson et al., 2008; Ameli et al., 2009; Talelli et al., 2012), yet the underlying mechanisms remain uncler.

Post-stroke hyperexcitability of surviving neurons contributes to the transient low-frequency (~ 1 Hz, 200-500 ms in duration), high amplitude, rhythmic waves (also coined 'bistable state') originating in the peri-infarct zone and propagating to contra-lesional brain areas. This distinctive 1-Hz slow and synchronous neural activity in the peri-infarct zone shares similarities with slow waves (SW) typically recorded during non-rapid eye movement (NREM) sleep in rodents and human. Indeed, SW reflect bistable states of thalamocortical neuron populations, described as a switch between UP states where depolarised membrane potentials are accompanied by high spiking activity, and DOWN states during which cells are hyperpolarized and show low spiking activities in cats (Steriade et al., 1993), rodents (Vyazovskiy et al., 2009; Zucca et al., 2017), non-human primates (Xu et al., 2019) and human (Csercsa et al., 2010). These SW were hypothesized to guide axonal sprouting and

104 circuit rewiring through the formation of new connections after brain lesions (Carmichael and
105 Chesselet, 2002) facilitating recovery, however this has not been directly demonstrated.
106
107 Extensive experimental evidence suggests a fundamental role for intact sleep, and SW in
108 particular, in enhancing brain plasticity during spontaneous sleep (Tononi and Cirelli, 2016;
109 Timofeev and Chauvette, 2017) and stroke recovery (Duss et al., 2017). The detrimental
110 effects of sleep disturbances (Kaneko et al., 2003; Baglioni et al., 2016) and the beneficial
111 effect of pharmacological NREM sleep enhancement after stroke support the hypothesis that
112 SW contribute to brain plasticity underlying post-stroke functional and cognitive recovery
113 both in animal models (Gao et al., 2008; Hodor et al., 2014) and patients (Vock et al., 2002;
114 Siccoli et al., 2008; Sarasso et al., 2014).
115
116 Here, we used an optogenetic approach inspired by global and local SW changes after stroke
117 to rescue SW-like activity in freely-moving mice. Optogenetic activation of pyramidal
118 neurons in the peri-infarct zone during NREM sleep improved fine motor movements as
119 compared to experimental control conditions. In contrast, optogenetically-evoked SW
120 (SW^{opto}) during wakefulness had no effect. Importantly, SW^{opto} evoked recovery after stroke
121 was associated with axonal sprouting in the peri-infarct zone and corresponding contra-
122 lesional areas.
123
124

125 # MATERIALS AND METHODS

126 **Animals**

127 C57BL/6JRj male mice (https://www.janvier-labs.com/en/fiche_produit/c57bl-6jrj_mouse/)
128 (5-6 weeks old, 23-30 grams) were used in the study. Animals were individually housed in

129 custom-designed polycarbonate cages (300 mm x 170 mm) under controlled conditions
130 (regular circadian cycle of 12:12 h light:dark; light on at either 4 a.m. or 8 p.m. according to
131 experimental design; constant temperature 22 ± 1 °C and humidity 30-50%). Throughout the
132 experiment animals were freely-moving with *ad libitum* food and water. Animals were kept
133 in groups of 2-5 per IVC cage before instrumentation and after viral injection surgery.
134 Following implantation mice were all housed individually. Animals were tethered, allowed to
135 adapt to the EEG/EMG and optic stimulation cables in their home cage for at least 5-7 days,
136 and remained plugged for the duration of the experiment. Animals were detached from all
137 tethers for 4 days following stroke or sham surgery and for the duration of behavioural
138 testing. Animals were randomly assigned to eight experimental groups: Channelrhodopsin
139 (ChR2) transfected animals subjected to stroke ($ChR2^{stroke}$), ChR2 transfected animals
140 subjected to stroke and optogenetically stimulated mainly during wakefulness
141 ($ChR2^{stroke\_wake}$), Archaerhodopsin (ArchT) transfected animals subjected to stroke
142 ($ArchT^{stroke}$), mCherry transfected animals subjected to stroke ($mCherry^{stroke}$), mCherry
143 transfected animals subjected to sham surgery ($mCherry^{sham}$), Naive, Sham and Stroke.
144 Animals that displayed baseline asymmetry in limb usage or did not show a drop in cerebral
145 blood flow (CBF) by ~ 80% during middle cerebral artery occlusion (MCAo) surgery were
146 excluded from further experimental tests. Viral injections were performed when animals were
147 5-6 weeks of age, instrumentation at 8 weeks of age and stroke/ sham surgery at 10 weeks of
148 age. Between surgeries and before being tethered, animals were let recover undisturbed for at
149 least 7 days. Naive mice did not undergo any surgical procedures. An additional set of
150 heterozygous Tg(VGAT-Cre) mice, (5-6 weeks old, 23-30 grams) was used for an
151 optogenetic screening of slow waves-like oscillations inducing protocols. All animals were
152 treated according to animal care laws and experimental procedures were approved by local

153 authorities (Veterinary Office, Canton of Bern, Switzerland; licence numbers BE 113/13 and
154 BE 41/17).
155

156 **Viral targeting**

157 For a detailed description of the surgical procedure refer to Herrera et al., 2016. Briefly, 5-6
158 weeks old animals were anesthetized with isoflurane (4.0% induction; 1.0-1.5%
159 maintenance). Body temperature was constantly monitored and kept at physiological range
160 using a rectal thermoprobe and feedback-controlled heating system. Animals were fixed in a
161 digital stereotaxic frame and analgesia was administered subcutaneously (Meloxicam,
162 5mg/kg). Animals were randomly assigned to receive 0.6 µL of recombinant AAV carrying
163 either CaMKII-hChR2 (H134)-EYFP (activation), CaMKIIa-eArchT3.0-EYFP (silencing) or
164 CaMKIIa-mCherry (control) respectively. Plasmids were stereotactically injected (0.1
165 µL/min infusion rate) through a 28 G needle (Plastic One), connected by a tubing to a 10 µL
166 Hamilton syringe in an infusion pump (Model 1200, Harvard Apparatus). Injections were
167 performed within the left (prospective ipsilateral) primary somatosensory forelimb cortex
168 (iS1FL, AP: -0.10 mm; ML: -2.00 mm; DV: -0.7 mm). Animals were given 7 days of
169 recovery prior to instrumentation surgery. Tg(VGAT:Cre) mice underwent identical surgical
170 procedures as wild type animals, randomly assigned to receive 0.6 µL of recombinant AVV
171 carrying Ef1α-DIO-ChR2-EYFP (activation), Ef1α-DIO-ArchT-EYFP (silencing) or Ef1α-
172 DIO-EYFP (control) respectively. All plasmids were obtained from the University of North
173 Carolina Vector Core Facility. Mice belonging to Sham, Stroke and Naive groups did not
174 received any AAV injection.
175

176 **Instrumentation**

Animals were chronically implanted with a unilateral optic fiber (200 µm in diameter) within the iS1FL (AP: -0.10 mm; ML: -2.00 mm; DV: -0.5 mm) and an electroencephalography (EEG)/electromyography (EMG) connector. As previously reported (Gent et al., 2018), animals received analgesia (Meloxicam, 5mg/kg), were anaesthetised with isoflurane and anchored to a stereotaxic frame. Five stainless steel EEG electrode screws were inserted through each animal's skull; two screws over the frontal cortices (AP: +2 mm; ML: ±2mm), two screws over the posterior cortices (AP: -4 mm; ML: ±2 mm) and one screw over the olfactory bulb as ground. For the stimulation recordings, the EEG signals from the frontal and posterior channels were referenced to each other directly, leaving only two EEG traces, one per hemisphere. Finally, two bare-ended EMG wires were sutured to the neck muscles to record postural tone. A subset of animals was additionally implanted with four tetrodes to record local field potentials (LFPs) and single unit activity during optogenetic stimulation, as well as EEG/EMG signals. Tetrodes were constructed by twisting four tungsten wires together (10 µm in diameter, CFW0010954, California Fine Wire) and briefly heating them to favour the bond coating of each wire to another. Tetrodes were lowered within the iS1FL (AP: -0.10 mm; ML: -2.00 mm; DV: -0.5 mm), the ipsilateral primary motor cortex (iM1, AP: +1.10 mm; ML: -1.5 mm; DV: -1.20 mm), the contralateral S1FL (cS1FL, AP: -0.10 mm; ML: +2.00 mm; DV: -0.5 mm) and the contralateral M1 (cM1, AP: +1.10 mm; ML: +1.5 mm; DV: -1.20 mm) respectively. The tetrode positioned in iS1FL was glued to the optic fiber, where the tip of the tetrode extended for ~ 0.2 mm beyond the end of the fiber (optrode). Optic fibers and implants were permanently secured to the skull with C&B Metabond (Patterson Dental) and methacrylate cement (Paladur). Animals were monitored post-operatively and left to recover undisturbed for at least 7 days. Animals were then plugged to the EEG/EMG/optic stimulation and tetrodes tethers (Neuralynx headstage). Black nail polish was applied at the connection point between optic fiber and patch cord to

limit laser light spreading during optogenetic stimulations. The implantation procedure for animals belonging to Sham and Stroke groups did not include either optic fiber or tetrodes placement.

Transient focal cerebral ischemic stroke

Mice underwent MCAo via intraluminal filament model (Doeppner et al., 2010) at around 10 weeks of age. To begin, mice were anaesthetised with isoflurane as previously described and placed in a prone position. Physiological temperature was maintained as mentioned above. The left common carotid artery (CCA) was dissected from the surrounding connective tissue. A monofilament suture (7-0 silicon rubber coated, coating length 5-6 mm, Doccol Corporation) was inserted in the CCA and introduced into the lumen of the MCA. The monofilament was left in place for 45 min to induce both striatal and cortical infarct and consequently withdrawn to allow the reperfusion of the territory targeted by the MCA. CBF was constantly monitored by a Laser Doppler probe (Moor Instrument, VMS-LDF2) glued to the skull above the MCA region. Ischemic stroke induction was considered successful when the CBF showed a ~ 80 % reduction from baseline values, as well as reperfusion of the MCA territory. Following surgery, mice were daily checked for pain and weight loss, received mashed, watered food, subcutaneous analgesia and 0.9% saline. Animals belonging to the Naive group did not undergo stroke or sham surgery. No filament was inserted into the MCA during sham surgery. Following MCAo, 40% of animals assigned to the Stroke group and 33% of all animals allocated to optogenetic stimulations did not survive the post-operation phase.

Optogenetic stimulation

Lasers (Laserglow Technologies) attached to the unilateral fiber via patch cord (Thorlabs) were triggered through TTL with a pulse stimulator (Master - 9, AMPI), this latter controlled by a function generator (Agilent, 33220A 20MHz Function/ Arbitrary Waveform Generator) to induce random pulse sequences. Animals received daily 2 h of randomly distributed single laser light pulses (inter-pulses interval 3-30 sec), from post-stroke day 5 until day 15. The random distribution of light pulses was selected to avoid hypersynchrony and entrainment of oscillatory activities which, *per se*, might influence the observed parameters. The optogenetic stimulation was semi-chronic: light pulses were distributed across sleep and wake states without simultaneous behavioural scoring by the experimenter and consequent state specific stimulation. Indeed, daily and chronic stimulation (11 days) of several animals (experimental and control were run in parallel) is not suited for a single experimenter. The specific time allocated for optogenetic intervention was therefore selected according to the natural distribution of the majority of NREM sleep and wakefulness episodes throughout the 12h light:dark cycle of the animals. Two stimulation protocols were employed: ChR2-expressing animals received 5 ms blue light pulses (473 nm wavelength), ArchT-expressing mice were stimulated with 200 ms green light pulses (532 nm wavelength) and mCherry-expressing animals were randomly subjected to either 200 ms or 5 ms light pulses. To assess whether the effect of SW^{opto} on functional recovery was specific to brain activity occurring during sleep, in a separate group of animals ($ChR2^{stroke\_wake}$) optogenetic stimulations were also delivered during the first part of the dark phase, when animals were mostly awake. Based on pre-instrumentation testing of both optic fiber and patch cord outputs, light power was set at 20-25 mW.

Data acquisition

EEG and EMG signals were amplified (Model 3500, AM System) and digitized at 512 Hz (NIDAQ 6363, National Instruments) using a sleep recording software (MATLAB written software, DaqReverse). A 24 h baseline of spontaneous sleep-wake behaviour was recorded for all animals. Stroke and Sham animals were recorded for 24 h at post-surgery days 1, 3, 5 and 10. All optogenetic stimulations took place between 9 a.m. and 2 p.m., with light on at 4 a.m. for $ChR2^{stroke}$, $ArchT^{stroke}$, $mCherry^{stroke}$ and $mCherry^{sham}$. Since $ChR2^{stroke}$ and $ArchT^{stroke}$ animals showed similar functional outcomes upon neuronal manipulation during sleep, an additional ChR2-transfected set of animals received SW^{opto} during animals' active phase (between 9 a.m. and 2 p.m., lights on at 8 p.m, $ChR2^{stroke\_wake}$), from post-stroke day 5 until day 15. Animals' spontaneous sleep was recorded for 18 h at post-stroke day 5, 6, 8, 12 and 14 respectively. LFPs and EEG/EMG signals were amplified and digitized at 32 kHz (Cheetah 5 acquisition software, Neuralynx, https://neuralynx.com/software/cheetah-5.0-legacy).

Behavioural tests

All animals were trained in four behavioural tests and engaged in daily training sessions for three consecutive days. Behavioural baselines were acquired prior to stroke/ sham surgery. Functional outcomes were verified at post-stroke days 4, 7, 10 and 15. All behavioural tests were conducted at least 3 h apart from optogenetic stimulations and during animals' active phase (between 5 p.m. and 8 p.m.). Test sessions were recorded with a picamera (Raspberry Pi) and scored in slow motion (VideoPad software, https://www.nchsoftware.com/videopad/index.html).

Balance beam test: To assess motor balance and coordination (Brooks and Dunnett, 2009) a round wooden beam (12 mm in diameter, 80 cm long) was positioned at an angle so that one end of the beam was 60 cm elevated from the working table. At the beam's elevated end, the

animal's home cage served as motivation to complete the task. Soft fabric placed beneath the beam avoided possible falling injuries. The number of 'paw faults' (forelimb or hindlimb slipping off the beam) were counted during a maximal testing time of 60 sec. Each animal underwent three trials per time point and means were calculated.

Tight rope test

To measure grip strength and endurance (Balkaya et al., 2013) animals were suspended on a fine rope (60 cm above the working table) between two platforms (80 cm apart from one another). Mice were positioned at the middle point of the rope exclusively with their forepaws. The average time needed to reach one of the two platforms was calculated between two trials. The maximum testing time was 60 sec.

Corner turn test

To evaluate the presence of unilateral abnormalities (Park et al., 2014) mice where placed in between two vertical boards forming a 30° angle. Animals left- or right-turn decision was recorded for a total of 10 trials per testing session. Laterality index was calculated as (number of left turns – number of right turns)/10.

Ladder walking rig test

The test was chosen to measure paw accurate placement (Cummings et al., 2007). The apparatus consisted of a ladder (80 cm long), suspended between two platforms (60 cm above the working table) with randomly spaced rungs. Paw faults were recorded as animals walked to reach the home cage at one end of the ladder. Mice performances were scored in slow motion and the mean of three trials calculated. The position of the rungs was randomly changed across trials to avoid learning.

Signal processing

As previously described (Jego et al., 2013), electrophysiological data were manually scored in 5 sec epochs and analysed using SlipAnalysis (custom written MATLAB program). Briefly, three vigilance state were identified based on EEG/EMG frequency and amplitude. Wakefulness was determined by low amplitude EEG and high activity EMG signals; NREM sleep as high amplitude and low-frequency EEG (0.5-4 Hz) paired with reduced EMG activity; REM was characterized by theta rhythm (6-9 Hz) EEG and flat EMG. Microarousals were defined and scored as cortical fast rhythm and EMG bursts of at least 1 sec. Sleep/ wakefulness scoring was based on the visual characteristics of the contralateral EEG traces specifically. Electrophysiological analysis was completed using custom MATLAB scripts.

Automatic single SW detection

Individual SW were detected during NREM sleep epochs during the first 7 h of the lights ON period in MATLAB using the SWA-MATLAB toolbox (Mensen et al., 2016), with detection parameters adjusted to rodents from settings described in Panagiotou et al., 2017. Briefly, in a first-pass of the data, the negative envelope across the 4 EEG channels was calculated, filtered between 0.5 and 4 Hz (Chebyshev Type II filter design), and consecutive zero-crossings were detected. If the duration between successive downward (negative going) zero-crossing and upward zero-crossing was between 100 msec and 1 sec, then the peak negative amplitude was examined and was required to be at least 3 deviations from the median amplitude of all negative peaks in the recording. The amplitude threshold eliminates the potential individual differences of electrodes reference type, distance to those reference, and electrode depth that would affect the record amplitude. In a second-pass, the activity over all 4 channels was examined for each slow wave detected on the negative envelope to obtain individual channel data.

Single unit analysis

We performed spike detection and sorting as described previously (Gent et al., 2018). Briefly, we first extracted multiunit activity from band-pass filtered signals (600-4000 Hz, 4^{th}-order elliptic filter, 0.1 dB passband ripple, -40 dB stopband attenuation), by applying a detection threshold of 7.5 × the median of the absolute values of the filtered signal. We then extracted wavelet coefficients from the detected multiunit activity using a four-level discrete wavelet transform (Harr wavelet, 'wavedec', MATLAB), and subsequently sorted the coefficients using the super-paramagnetic clustering. We visually inspected the sorted units and excluded the clusters with a symmetric shape or an average firing rate less than 0.2 Hz from our analyses.

Optogenetic response analysis

We assessed the optogenetic response analysis for each vigilance state separately. For unit activity, we calculated mean firing rates during optogenetic perturbations by averaging firing rates across trials using a non-overlapping moving window of 5 ms. For LFP analysis, we averaged raw LFP signals across trials of each vigilance state.

Infarct volume evaluation and immunohistochemistry

Animals were sacrificed at post-stroke day 15 with 15 mg pentobarbital intraperitoneal injection (Esconarkon ad us. vet., Streuli Pharma) and transcardially perfused with 1x phosphate buffered saline (PBS) followed by 4% formalin. Brains were post-fixed overnight, cryoprotected in 30% sucrose (24-48 h at 4°C), frozen in 2-methyl-butane on dry ice and cut into 40 µm sections. Every third slice was mounted onto a glass slide, dried at room temperature (RT), rehydrated and processed for Nissl staining. Briefly, sections were immersed in Cresyl Violet (Klüver Barrera, Bio-Optica), washed in distilled water and

dehydrated in graded alcohols, cleared in Xylene (Sigma-Aldrich) and mounted (Eukitt mounting medium, Bio-Optica) on microscope slides. Stroke edges were delineated per section using Imagej software (https://imagej.nih.gov/ij/). The damaged area was measured in each brain slice and multiplied by the distance between brain sections. Stroke volume relative to the whole brain was calculated as follows: ((volume of contralesional hemisphere - volume of ipsilesional hemisphere)/2 * volume of contralesional hemisphere) * 100 (Lin et al., 1993). Fluorescent immunohistochemical staining was performed with free-floating brain sections. Brain slices were washed in PBS-Triton (PBS-T) and incubated in blocking solution (1 h at RT; PBS-T with 4% of bovine serum albumin, SIGMA Life Science). Free-floating slices from ChR2- and ArchT-expressing animals were incubated in a primary antibody to GFP (chicken IgY fraction anti-GFP, 1:5000, Cat# A10262, RRID:AB_2534023, Life Technologies) in blocking solution (24-48 h at 4°C). Following repeated washes in PBS-T, sections were incubated with the secondary antibody (1:500, Cat# ab96947, RRID:AB_10681017, Abcam) in PBS-T (1 h at RT). Sections were then washed in PBS-T, mounted and covered on microscope slides.

Axonal sprouting quantification

Four brains per experimental group were randomly chosen for axonal sprouting evaluation. Brains were fixed, frozen and cut as previously described. Several 40 µm sections per brain were selected (approximately, from Bregma 1.10 mm to Bregma -0.70 mm) and stained for Vglut1, PSD-95 and DAPI. Floating sections were washed in PBS and blocked in PBS with 0.5% Triton X-100 and 10% normal donkey serum (NDS, Jakson ImmunoResearch Code: 017-000-121) (2 h at RT). Sections were then incubated with the following primary antibodies: chicken IgY fraction anti-GFP ($ChR2^{stroke}$ and $ArchT^{stroke}$, Cat# A10262, RRID:AB_2534023, Life Technologies), rabbit anti-Vglut1 ($ChR2^{stroke}$, $ArchT^{stroke}$, mCherry-

expressing animals, 1:1000, Cat# 135 303, RRID:AB_887875, SYSY), goat anti-PSD-95 ($ChR2^{stroke}$, $ArchT^{stroke}$, mCherry-expressing animals , 1:500, Cat# ab12093, RRID:AB_298846, Abcam) and mCherry respectively (mCherry-expressing animals, 1:1000, Cat# M11217, RRID:AB_2536611, Life Technologies) in PBS containing 3% NDS and 0.5% Triton X-100 solution (overnight at 4°C). Brain slices were repeatedly washed in PBS and incubated with appropriate secondary antibodies (1:500, Alexa Fluor 488 Ab96947, Abcam; all others 1:1000, Invitrogen) in PBS containing 3% NDS and 0.5% Triton X-100 solution (2 h at RT). A negative control (no addition of primary antibody) was carried out to confirm the antibody selectivity. Sections were further stained for DAPI (1:500 in PBS, 10 minutes), washed in PBS, mounted on microscope slides and covered. Photomicrographs were acquired with Olympus Fluoview 1000-BX61 confocal microscope (Olympus, Tokyo) fitted with 60X oil-immersion objective (4x zoom, 0.5 µm step size). Three fields of interest (52.172 µm x 52.172 µm) within iS1FL and cS1FLwere imaged in three sections per animal. Imaris software (Microscopy Image Analysis Software, Bitplane, https://imaris.oxinst.com/) was used to reconstruct the 3D view of the Z stacks and to evaluate pre- and post- synaptic compartments' density and volume. Briefly, background subtraction, image smoothing via gaussian filtering and channel intensity adjustment were applied and maintained identical for all the acquired confocal images. A preliminary stack selection was carried out to localize pucta distributed within two consecutive stacks. A puncta diameter threshold was specified at 0.6 µm and when this value was exceeded, puncta were separated upon visual confirmation by the experimenter.

Statistical analysis

For the analyses of the 24 h recordings of stroke and sham animals, a two-level analysis was performed using linear mixed models. A first-level analysis on each animal and recording

399 day, including temporal predictors of recording time, time since last wake epoch in order to
400 estimate the homeostatic effect on individual slow wave characteristics across the lights on
401 period as well as the potential differences between the ipsi- and contralateral hemisphere. At
402 the second level, the parameter estimates from the first level data for each animal for each
403 day were used to examine the overall effects of stroke over the course of 10 days after stroke.
404 The potential effects of days, stroke, stimulation group, on sleep parameters and behavioural
405 outcomes were tested using linear mixed models. Sleep and behavioural values from day 0
406 was assigned as a baseline predictor, while those from day 4 were used as pre-stimulation
407 baseline. Main effects and interactions were tested for significance using the log-likelihood
408 ratio test between the full model and the model without the specific factor in question. The
409 effects between the stimulation groups were examined by post-hoc t-tests within the linear
410 mixed model. As an exploratory analysis, macro and micro sleep parameters during the
411 stimulation time were included as a potential predictor of behavioural outcome: percentage of
412 NREM, number of micro-arousals, NREM-to-wake transition ratio, wave incidence, wave
413 amplitude, wave duration, positive and negative slope.
414 For the pre- and post-synaptic markers assessment, statistical comparisons were determined
415 with Student's *t*-test, one-way ANOVA, where corrections for multiple comparisons were
416 carried out using Bonferroni correction, if not otherwise indicated (Prism 6 GraphPad;
417 https://www.graphpad.com/scientific-software/prism/). Data are presented as mean ± standard
418 error of the mean (s.e.m.) and levels of statistical significance were set at threshold $p < 0.05$
419 unless otherwise indicated. Sample sizes were defined based on previous studies (Gao et al.,
420 2008; Jego et al., 2013; Herrera et al., 2016). For each experiment, sample numbers are
421 indicated in the corresponding figure legends. Animals that did not perform behavioural
422 testing were excluded from the analysis; as well as mice that lost EEG/EMG signals during
423 longitudinal measurements. Data distribution was tested for normality using the Lilliefors test

on the residuals from each linear mixed model calculated and found to be normally distributed. Experiments were not conducted in blinded fashion.

Data availability

Dataset and coding supporting the current study are available from the corresponding author upon request.

RESULTS

Stroke alters sleep architecture and SW profile

SWs-like oscillations are frequently observed in peri-infarct zone during NREM sleep and wakefulness (Yokoyama et al., 1996; Murri et al., 1998; Fernandez-Bouzas et al., 2002). To refine the characterization of brain activity after stroke, including SW features, we first quantified the changes of sleep-wake architecture and sleep quality from animals subjected to MCAo and sham surgeries (Fig. 1A, B). Animals were chronically implanted with EEG/EMG electrodes for longitudinal sleep recordings prior to, and at 1, 3, 5, and 10 days after MCAo (see Methods; Fig. 1C). To control for multiple comparisons between the 8 sleep metrics, the significance threshold was reduced to $p < 0.0063$ (i.e. 0.05/8; Bonferroni correction). MCAo resulted in an initial increase of NREM sleep duration with group differences dampening over the days recorded (Figure 1E, *Day* by *Stroke* interaction: $LR(1) = 7.977$, $p = 0.0047$). Significant main effects of stroke were found for total wake duration (Figure 1D; $LR(2) = 22.385$, $p < 0.0001$); and wake bout duration ($LR(2) = 34.502$, $p < 0.0001$), but this general effect was not significantly different over the days after correction (*Day* by *Stroke* interaction: $LR(1) = 4.328$, $p = 0.0375$). No significant results were observed for REM sleep total duration (Fig. 1F). We further explored the potential effect of stroke size

449 within the MCAo group on all sleep architecture measures but found no main effects or
450 interaction effects with the day of recording (all p-values > 0.0063).
451 NREM sleep instability, describing the ratio between the animals' capacity of remaining
452 asleep compared to waking up, showed that stroke animals were significantly more likely to
453 wake up (Fig. 1J; LR(2) = 14.918, p = 0.0006).
454 The number of microarousals, scored as single epoch of 1 sec (minimum) increased EMG
455 signal within a NREM sleep episode, did not differ between Stroke and Sham (Fig. 1K;
456 LR(2) = 4.651, p = 0.0977).
457
458 To assess SW features and changes after MCAo stroke, animals were prepared for
459 simultaneous recordings of EEG/EMG, LFPs or single/ multi-units activities in iS1FL,
460 cS1FL, iM1 and cM1 layer V (see Methods and Fig. 2B for illustration). Clear periods of
461 neuronal quiescence corresponding to cortical DOWN states confirmed the selectivity of our
462 SW detection method (see Methods for detection criteria; Fig. 2A-D). Indeed, perilesional
463 tetrodes recordings of unit activity in S1FL showed suppression, and subsequent increase, in
464 neuronal activity (Fig. 2D, top), validating the average unit firing rate observed during the
465 detected SW (Fig. 2D, bottom). Both local and global SW occurred across all recorded
466 neocortical areas (Fig. 2A), consistent with previous reports in rodents and humans (Huber et
467 al., 2004; Vyazovskiy et al., 2011). If individual waves are detected across the 24 h period,
468 we observed a significant reduction of ipsilateral SW's amplitude by -13.2 ± 7.3% after
469 stroke as compared to sham controls that persisted for up to 10 days after stroke (Fig. 2F; day
470 10: -15.4 ± 6.4%; F(2, 70) = 13.82, p < 0.0001; two-way ANOVA, followed by Bonferroni
471 post-hoc test). These findings are consistent with hemispheric stroke in rodents and human
472 subjects (Ahmed et al., 2011; Poryazova et al., 2015). Moreover, the SW positive slope was
473 reduced within the ipsilateral area of Stroke animals (Fig. 2G; F(2, 76) = 13.02, p < 0.0001),

whereas the negative slope increased (Fig. 2H; $F(2, 76) = 15.89$, $p < 0.0001$). No significant changes were found in the number of detected SW (Fig. 2I; $F(2, 87) = 0.693$, $p = 0.503$) or their duration (Fig. 2J; $F(82, 83) = 0.744$, $p = 0.478$; two-way ANOVA, followed by Tukey post-hoc test). When exploring for a homeostatic effect, we did not find differences in amplitude between Stroke and Sham for ipsi- and contralateral EEG traces ($LR(2) = 0.940$, $p = 0.625$) nor for *time of night* ($LR(2) = 3.791$, $p = 0.150$).

SW^{opto} revealed a critical window of intervention after stroke

Here, we aimed at identifying the effect of optogenetically-induced SW ($SW^{opto)}$ on the recovery of motor function following MCAo stroke in mice. Thus, we genetically targeted the expression of opsins to pyramidal neurons in layer V of the neocortex, given their implication in the generation of slow oscillations (McCormick et al., 2015; Beltramo et al., 2013). To achieve this, we stereotactically infused AAV2 viruses carrying ChR2, ArchT or mCherry gene cassettes under CaMKII promoter in iS1FL (Fig. 3A, B) before animals were chronically implanted with EEG/EMG electrodes, tetrodes in cS1FL, iM1 and cM1 cortices (layer V) and a single optrode in iS1FL (see above and Methods, Fig. 3A). We first optimized the frequency and duration of optogenetic stimulations to mimic NREM sleep SW in both wild type and VGAT-Cre transgenic mice to modulate excitatory or inhibitory neurons in iS1FL with 5 Hz, 1 ms light pulses (activation protocol) or 100, 200, 500 ms single pulses (silencing protocol) (Fig. 4). We found that 5 ms optogenetic activation of iS1FL ChR2-expressing pyramidal neurons induced a short UP-like state followed by a DOWN-like state, indistinguishable from spontaneous NREM sleep SW (Fig. 3C-E). Similar SW^{opto} waveform profiles were obtained upon 200 ms optogenetic silencing of iS1FL ArchT-expressing pyramidal neurons (Fig. 3F, I). In the latter condition, the duration of the optogenetic silencing of iS1FL ArchT-expressing pyramidal neurons corresponded to the average

duration of spontaneous NREM sleep DOWN states (Fig. 2C; duration: 205.2 ± 4.4 ms; Fig. 3H). Off-line analysis confirmed that SW^{opto} duration, negative amplitude and slope were indistinguishable from naturally occurring NREM sleep SW from the same animal (Fig. 3E, I). SW^{opto} propagated to contralateral recording sites, where SW^{opto} of variable amplitudes were recorded in EEG, LFP and single activity traces (Fig. 3D, H and Fig. 5). No changes in EEG features were observed in control conditions (Fig. 3J-L).

To determine the optimal window for optogenetic intervention after MCAo, we evaluated the effect of this stimulation parameters on the survival rates of stroke animals. Strikingly, we observed that $ChR2^{stroke}$ animals had lower survival rate than $ArchT^{stroke}$ and $mCherry^{stroke}$ mice when the optogenetic manipulation started on post-stroke day 1 (single 5 or 200 ms light pulses, at 473 nm or 532 nm, respectively, randomly distributed over 2 h, daily; Fig. 6A; Chi square(2) = 7.941, p = 0.018; $ChR2^{stroke}$: 30% survival; $ArchT^{stroke}$: 75% survival; $mCherry^{stroke}$: 77.7% survival; Log-rank Mantel-Cox test), as compared to day 5 (Fig. 6B; Chi square(4) = 6.383, P = 0.172; $ChR2^{stroke}$: 60% survival; $ArchT^{stroke}$: 70% survival; $mCherry^{stroke}$: 70% survival; $mCherry^{sham}$: 100 % survival; Naive: 100 % survival; Long-rank Mantel-Cox test). These findings are consistent with an increased excitotoxicity after stroke (Nudo, 2006; Allman et al., 2016), hence, all our optogenetic experiments started on day 5.

SW^{opto} during sleep improves functional recovery

We next tested whether sleep-specific SW^{opto} improves functional recovery after MCAo in mice. The expression of ChR2, ArchT and mCherry was genetically targeted to iS1FL pyramidal neurons as described above (Fig. 3A) before animals were chronically implanted with a unilateral optic fiber on iS1FL and EEG/EMG electrodes for simultaneous optogenetic control and polysomnographic recordings in freely moving mice (Fig. 7A; see Methods).

Sparse SW^{opto} were randomly distributed during sleep starting 5 days after stroke until day 15 (single 5 or 200 ms light pulses, at 473 nm or 532 nm, respectively, randomly distributed over 2 h, daily; n =~300 optical stimuli; Fig. 7B, C).

Evaluation of the animals' fine motor movements, coordination, strength and asymmetry at post-stroke day 4 (Fig. 7B) showed severe behavioural deficits in all animals subjected to MCAo. Indeed, on post-stroke day 4 stroke-induced animals were no longer able to finely coordinate their grasping movements (Fig. 7D; $LR(1) = 27.498$, $p < 0.0001$; Fig. 7F; $LR(1) = 32.205$, $p < 0.0001$). As expected, no behavioural impairments were found in $mCherry^{sham}$ and Naive animals (Fig. 7D; F, respectively, $p > 0.05$).

In the ladder walking rig test (Fig. 7D), a significant interaction between the *stimulation group* and *days* was found ($LR(5) = 11.976$, $p = 0.035$). Post-hoc analysis revealed that the $ArchT^{stroke}$ group recovered at a faster pace than $ChR2^{stroke\_wake}$ ($t(101) = 2.842$, $p = 0.005$). Generally all mice improved across days ($LR(6) = 28.235$, $p < 0.001$). Main effects of stimulation group were also found ($LR(10) = 42.949$, $p < 0.001$). $ChR2^{stroke}$, $ChR2^{stroke\_wake}$ were significantly different from $mCherry^{stroke}$ ($t(101) = -2.430$, $p = 0.017$; $t(101) = -3.137$, $p = 0.002$). For the beam balance (Fig. 7F) we found a significant interaction effect of *stimulation group* and *day* ($LR(5) = 14.171$, $p = 0.015$). $mCherry^{stroke}$ did not show a significant improvement across days ($t(152) = -1.671$, $p = 0.097$). However, compared to $mCherry^{stroke}$, $Archt^{stroke}$ mice showed significantly more improvement over the course of days ($t(110) = -2.866$, $p = 0.005$). $ChR2^{stroke}$ mice also significantly improved across days after stroke ($t(152) = -4{,}168$, $p < 0.001$), but this improvement was less than the $ArchT^{stroke}$ group ($t(110) = -2.285$, $p = 0.024$) and on par with the $mCherry^{stroke}$ group ($t(110) = 0.580$, $p = 0.563$). Comparisons of animal improvement between post-stroke day 4 and 15 confirmed the functional recovery of $ChR2^{stroke}$ (Fig. 7E; $t(14) = 3.46$, $p = 0.007$; Fig. 7G; $t(18) = 2.372$,

549 p = 0.029) and ArchT^{stroke} (Fig. 7E; t(14) = 3.083, p = 0.008; Fig. 7G; t(18) = 3.895 p =
550 0.002; one-way ANOVA), in comparison to mCherry^{stroke} control. In contrast, optogenetic
551 intervention after stroke did not lead to any improvement of motor endurance, strength (Fig.
552 7H) or asymmetry (Fig. 7I).
553
554 **SW^{opto} increases axonal sprouting**
555 Stroke triggers a cascade of molecular and cellular changes including synaptogenesis,
556 neurogenesis and axonal sprouting in peri-infarct zone and remote connected circuits (Nudo,
557 1997; Carmichael et al., 2017).
558 To quantify the anatomical changes induced by chronic SW^{opto}, we quantified the expression
559 of pre-synaptic Vglut1 and post-synaptic PSD-95 proteins as a direct measurement of axonal
560 sprouting in cortical layers V (Liu et al., 2007; Sun et al., 2017) and connected circuits in
561 layers II (Binzegger et al., 2004; Adesnik and Naka, 2018) (Fig. 8A). Puncta density
562 quantification in both iS1FL and cS1FL cortices revealed a significantly higher Vglut1
563 protein levels in ipsilateral layer II (Fig. 8B; F(3, 19) = 10.49, p = 0.0003), and layer V (Fig.
564 8C; F(3,18) = 16.02, p > 0.0001; one-way ANOVA) from ChR2^{stroke} and ArchT^{stroke} animals,
565 as compared to mCherry controls. Consistently, analysis of Vglut1 positive puncta volume
566 distribution revealed a significant increase of smaller, newly-formed puncta within ipsilateral
567 layer V of both ArchT^{stroke} and ChR2^{stroke} as compared to mCherry^{stroke} animals (Fig. 8E; F(2,
568 2111) = 75.13, p < 0.0001). This was also true for *ex novo* Vglut1 puncta in post-synaptic
569 sites of layer II from ChR2^{stroke} animals (Fig. 8D; mCherry^{stroke} vs. ChR2^{stroke} t(2070) = 4.181,
570 p < 0.0001), but not ArchT^{stroke} animals (mCherry^{stroke} vs. ArchT^{stroke} t(2070) = 3.015, p =
571 0.0078, ChR2^{stroke} vs. ArchT^{stroke} t(2070) = 0.903, p > 0.999; one-way ANOVA, followed by
572 Bonferroni correction).

These pre-synaptic changes were concomitant to a significant decrease of post-synaptic PSD-95 protein expression in iS1FL layer II of both ChR2 and ArchT expressing animals when compared to control group (Fig. 8F; $F(3, 23) = 8.609$, $p = 0.0005$; one-way ANOVA), with no differences in layer V (Fig. 8G; $F(3, 24) = 1.095$, $p = 0.370$; one-way ANOVA). PSD-95 positive puncta volume were significantly larger iS1FL layer II (Fig. 8H; $F(2, 625) = 85$, $p < 0.0001$) and layer V from $ChR2^{stroke}$ animal as compared to $mCherry^{stroke}$ or $ArchT^{stroke}$ (Fig. 8I; $(F(2, 2111) = 75.13)$, $p < 0.0001$; one-way ANOVA).

DISCUSSION

Stroke is a debilitating neurological disorder and one of the worldwide leading causes of adult disability and death in aging population. A better understanding of the complex pathophysiological mechanisms underlying the stroke event and the following brain plasticity warrants the improvement of existing strategies and the development of alternative therapies for stroke recovery (Feigin et al., 2017).

Here, we showed that MCAo induced an ipsilateral reduction of spontaneous SW amplitude, associated with sleep fragmentation and increased NREM sleep after stroke onset (Giubilei et al., 1992; Vock et al., 2002; Baumann et al., 2006; Hermann et al., 2008). Our results further indicate that sleep-specific optogenetic neuromodulation of brain activity after stroke had no effects on the sleep-wake cycle architecture, but it improved fine skilled motor movements in comparison to wakefulness interventions. These manipulations were accompanied by axonal sprouting of local and connected circuits, suggesting a direct role for SW in promoting anatomical and functional plasticity of neural circuit during sleep (Carmichael and Chesselet, 2002; Aeschbach et al., 2008; Tononi and Cirelli, 2014). Collectively, these findings emphasize a role for NREM sleep SW as a window of intervention during stroke recovery

598 and a possible mechanism underlying the improvement of rehabilitative strategies using
599 repetitive transcranial magnetic stimulation (rTMS) (Kim et al., 2006; Brodie et al., 2014)
600 and transcranial direct current stimulation (tDCS) (Boggio et al., 2006; Lindenberg et al.,
601 2010).

602

603 Spontaneous sleep SW are associated with neuroplastic changes (Tononi and Cirelli, 2006;
604 Puentes-Mestril and Aton, 2017), inflammatory and immunological adaptative response
605 (Irwin and Cole, 2011), protective functions during infection (Irwin, 2019), metabolic
606 clearance (Xie et al., 2013). Clinical studies reported significant improvement in stroke
607 rehabilitation upon non-invasive brain stimulation during sleep (Niimi et al., 2018) and SW
608 enhancement (Ebajemito et al., 2016). We used physiologically-relevant stimulation
609 protocols to avoid neuronal hypersynchrony, un-natural firing activities and circuit adaptation
610 by using single optogenetic stimuli randomly distributed across sleep in freely-moving
611 animals. These sparse optogenetics interventions induced SW^{opto} without perturbing sleep-
612 wake cycle architecture. Our strategy contrasts from other studies that use long-lasting
613 hypersynchronous optogenetic activation independently of the animal behaviour, sleep-wake
614 states, or delivered during anaesthesia (Cheng et al., 2014; Shah et al., 2017; Tennant et al.,
615 2017; Lu et al., 2017). Our findings show that sparse SW^{opto} delivered during sleep improved
616 behavioural outcomes whereas SW^{opto} during wakefulness did not. An explanation for this
617 striking difference is that low frequency, high amplitude waves during wakefulness represent
618 dysfunctional waves, typical of pathological conditions that are often associated with
619 functional abnormalities, including deafferentiated or lesioned thalamo-cortical circuits
620 (Steriade et al., 1993; Butz et al., 2004). These results further emphasize the importance of
621 sleep as a window for optimal modulation of brain activity that potentiates the effect of
622 SW^{opto} on brain plasticity and behavioural outcomes (see below).

623

624 ***Alteration of sleep-wake cycle and slow wave***

625 Our findings showed that stroke injury induces a dramatic increase in NREM sleep on the
626 day following stroke. This effect is accompanied by transient perturbation of the circadian
627 sleep distribution across the light/ dark cycle. Although the causes of these transient changes
628 remain unclear, they may result from a functional adaptation to the strong fragmentation of
629 both NREM sleep and wakefulness.

630 Our experimental results are consistent with the sleep fragmentation, the increase in NREM
631 sleep stages 1-2 and the decreased REM sleep observed during the first days following stroke
632 in human (Giubilei et al., 1992; Vock et al., 2002). Sleep fragmentation may result from a
633 lack of consolidated synchrony of neuronal activity amongst thalamo-cortical circuitries, as
634 suggested by the decreased amplitude and positive slope of spontaneous SW after stroke
635 observed in our study. These SW profiles are indicative of low spiking synchrony of thalamic
636 and cortical neurons (Huber et al., 2004; Vyazovskiy et al., 2009), which may facilitate
637 arousal upon wake-promoting inputs of sub-cortical origins (Adamantidis et al., 2007; Carter
638 et al., 2010; Herrera et al., 2016; Gent et al., 2018). Whether the SW remaining after stroke
639 are generated by a similar mechanism and support similar cortical functions, as the
640 naturalistic SW recorded from an intact brain remains to be examined in light of the different
641 cells types potentially implicated in SW generation (Gerashchenko et al., 2008; Cardin et al.,
642 2009; Stroh et al., 2013; Jackson et al., 2016; Niethard et al., 2016). An important
643 characteristic of spontaneous sleep SW is their propagation pattern across the brain cortex,
644 originating at anterior regions and travelling to posterior directions (Massimini et al., 2004,
645 Gent et al., 2018). Investigating SW's traveling changes across the ipsi-lateral hemisphere
646 and the peri-infarct zone specifically represents an interesting additional aspect to explore in

647 future work. The experimental preparation of the present study (single EEG trace per
648 hemisphere) limited further SW analysis in this direction.
649
650 ***SW^{opto} promotes behavioural recovery after stroke***
651 Chronic SW^{opto} over 11 days after stroke facilitated spontaneous functional recovery, while
652 earlier interventions exacerbated brain injury and decreased the survival rate of the animals,
653 possibly due to excessive glutamate release (Lai et al., 2014) leading to increased
654 excitotoxicity (Nudo, 2006; Allman et al., 2016). This window of spontaneous recovery is
655 limited to a month in rodents, and three months in humans, during which molecular and
656 structural changes potentiate the responsiveness to rehabilitative treatments (Murphy and
657 Corbett, 2009; Ng et al., 2015) and emphasize a crucial intervention timeframe (Dromerick et
658 al., 2009). Although post-stroke excitotoxicity might be an accurate explanation for the
659 detrimental effect observed in animals' survival, additional studies are required to further
660 scrutinize markers of excitotoxicity (e.g. levels of glutamate, NMDA receptors, AMPA
661 receptors and their activation, caspases, reactive oxygen species) in combination with
662 optogenetic intervention at several time points following stroke.
663
664 An interesting finding in our study is that SW^{opto} had no direct effects on sleep architecture
665 but induced a delayed increase of sleep duration. This result is in agreement with studies
666 showing prolonged NREM sleep upon activation of somatostatin interneurons (Funk et al.,
667 2017), and to a lesser extent pyramidal neurons (Rodriguez et al., 2016) in the neocortex.
668 Noteworthy, increased NREM sleep following SW^{opto} intervention was present only within
669 the first two days of stimulation (not shown), presumably due to the brain recovery processes
670 or the adaptation of the sleep-promoting circuits to the SW^{opto}, or both. Although we cannot
671 rule out a possible role of this transient NREM sleep increase on the sensorimotor

672 improvement of the animals, it is unlikely that these early and transient changes are
673 responsible for the motor improvements observed at the end of the experiment.
674
675 ***Slow wave, plasticity and axonal sprouting***
676 In our experiments, sensorimotor improvement after stroke was achieved by either chronic
677 optogenetic activation, or silencing, of iS1FL pyramidal neurons in freely-moving mice,
678 supporting an essential role for UP-DOWN states, rather than neuronal activation or silencing
679 alone, in brain plasticity (Puentes-Mestril and Aton, 2017). These bistable states during
680 NREM sleep (here, mainly SW^{opto}) are associated with synaptic plasticity in local circuits and
681 their postsynaptic targets, as observed for the beneficial effect of sleep low frequency
682 stimulation of motor or somatosensory cortical circuits on perceptual learning (Miyamoto et
683 al., 2016) or the formation of new dendritic spines in motor cortex (layer V) pyramidal
684 neurons in mice (Yang et al., 2014). Furthermore, our results are in agreement with the
685 finding that experimental disruption of cortical SW following learning impairs consolidation
686 of visuomotor learning in human (Landsness et al., 2009).
687
688 The early stages of stroke recovery are classically attributed to brain oedema resorption and
689 penumbra reperfusion, while later stages are associated with structural reorganization through
690 axonal sprouting, synaptogenesis and neurogenesis (Nudo, 2006). Here, both ChR2-, and to a
691 lesser extent ArchT-induced SW^{opto} promoted an increase of pre- and post-synaptic markers
692 in S1FL layers V and II respectively. Decreased PSD-95 density after SW^{opto} is consistent
693 with similar findings upon rTMS stimulation in rodents (Etiévant et al., 2015) that correlate
694 with improved functional outcomes in non-human primates treated with PSD-95 inhibitors
695 (Cook et al., 2012). Larger PSD-95 puncta were found within both layers II and V of
696 $ChR2^{stroke}$ animals, suggestive of a stabilization of the functional synapse (Cane et al., 2014).

Thus, SW^{opto} enhance UP/ DOWN state network synchronization (Gent et al., 2018) and facilitate the formation of new synapses which are not restricted to targeted cortical circuits (i.e. pyramidal neurons in the peri-infarct zone) but also anatomically connected circuits located in ipsi- and contra-lateral hemispheres (Liu et al., 2009; Cui et al., 2013). Noteworthy, brain activity in other cortical and sub-cortical networks and other sleep oscillations including spindles participate to synaptic plasticity during NREM sleep (Rosanova and Ulrich, 2005; Chauvette et al., 2012) and may contribute to the behavioral outcome reported here.

Collectively, our findings support a role for NREM sleep SW in neuronal circuit plasticity and provide a clinically-relevant framework for developing sparse, non-invasive neuromodulation, including acoustic brain stimulations (Ngo et al., 2013), TMS or tDCS (Ebajemito et al., 2016; Niimi et al., 2018) for optimal recovery after brain injury.

REFERENCES

Adamantidis AR, Zhang F, Aravanis AM, Deisseroth K, de Lecea L (2007) Neural substrates of awakening probed with optogenetic control of hypocretin neurons. Nature 450:420–424.

Adesnik H, Naka A (2018) Cracking the Function of Layers in the Sensory Cortex. Neuron 100:1028–1043.

Aeschbach D, Cutler AJ, Ronda JM (2008) A Role for Non-Rapid-Eye-Movement Sleep Homeostasis in Perceptual Learning. J Neurosci 28:2766–2772.

Ahmed S, Meng H, Liu T, Sutton BC, Opp MR, Borjigin J, Wang MM (2011) Ishcemic stroke selectively inhibits REM sleep if rats. Exp Neurol 232:168-75.

Allman C, Amadi U, Winkler AM, Wilkins L, Filippini N, Kischka U, Stagg CJ, Johansen-Berg H (2016) Ipsilesional anodal tDCS enhances the functional benefits of rehabilitation in patients after stroke. Sci Transl Med 8:1–21.

Ameli M, Grefkes C, Kemper F, Riegg FP, Rehme AK, Karbe H, Fink GR, Nowak DA (2009) Differential effects of high-frequency repetitive transcranial magnetic stimulation over ipsilesional primary motor cortex in cortical and subcortical middle cerebral artery stroke. Ann Neurol 66:298–309.

Asanuma H, Arissian K (1984) Experiments on functional role of peripheral input to motor cortex during voluntary movements in the monkey. J Neurophysiol 52:212–227.

Baglioni C, Nissen C, Schweinoch A, Riemann D, Spiegelhalder K, Berger M, Weiller C, Sterr A (2016) Polysomnographic characteristics of sleep in stroke: A Systematic review and meta- analysis. PLoS One 11:1–23.

Balkaya M, Kröber JM, Rex A, Endres M (2013) Assessing post-stroke behavior in mouse models of focal ischemia. J Cereb Blood Flow Metab 33:330–338.

Baumann CR, Kilic E, Petit B, Werth E, Hermann DM, Tafti M, Bassetti CL (2006) Sleep

736 EEG changes after middle cerebral artery infarcts in mice: Different effects of striatal
737 and cortical lesions. Sleep 29:1339–1344.
738 Beltramo R, D'Urso G, Dal Maschio M, Farisello P, Bovetti S, Clovis Y, Lassi G, Tucci V,
739 De Pietri Tonelli D, Fellin T (2013) Layer-specific excitatory circuits differentially
740 control recurrent network dynamics in the neocortex. Nat Neurosci 16:227–234.
741 Binzegger T, Douglas RJ, Martin KAC (2004) A Quantitative Map of the Circuit of Cat
742 Primary Visual Cortex. J Neurosci 24:8441–8453.
743 Boggio PS, Nunes A, Rigonatti SP, Nitsche MA, Pascual-Leone A, Fregni F (2006) Repeated
744 sessions of noninvasive brain DC stimulation is associated with motor function
745 improvement in stroke patients. Restor Neurol Neurosci 25:123–139.
746 Brochier T, Boudreau MJ, Paré M, Smith AM (1999) The effects of muscimol inactivation of
747 small regions of motor and somatosensory cortex on independent finger movements and
748 force control in the precision grip. Exp Brain Res 128:31–40.
749 Brodie SM, Meehan S, Borich MR, Boyd LA (2014) 5 Hz repetitive transcranial magnetic
750 stimulation over the ipsilesional sensory cortex enhances motor learning after stroke.
751 Front Hum Neurosci 8:1–10.
752 Brooks SP, Dunnett SB (2009) Tests to assess motor phenotype in mice: A user's guide. Nat
753 Rev Neurosci 10:519–529.
754 Butz M, Gross J, Timmermann L, Moll M, Freund HJ, Witte OW, Schnitzler A (2004)
755 Perilesional pathological oscillatory activity in the magnetoencephalogram of patients
756 with cortical brain lesions. Neurosci Lett 355:93–96.
757 Cane M, Maco B, Knott G, Holtmaat A (2014) The Relationship between PSD-95 Clustering
758 and Spine Stability In Vivo. J Neurosci 34:2075–2086.
759 Cardin JA, Carlén M, Meletis K, Knoblich U, Zhang F, Deisseroth K, Tsai LH, Moore CI
760 (2009) Driving fast-spiking cells induces gamma rhythm and controls sensory responses.

761 Nature 459:663–667.
762 Carmichael ST (2012) Brain excitability in stroke: The yin and yang of stroke progression.
763 Arch Neurol 69:161–167.
764 Carmichael ST, Chesselet M-F (2002) Synchronous neuronal activity is a signal for axonal
765 sprouting after cortical lesions in the adult. J Neurosci 22:6062–6070.
766 Carmichael ST, Kathirvelu B, Schweppe CA, Nie EH (2017) Molecular, cellular and
767 functional events in axonal sprouting after stroke. Exp Neurol 287:384–394.
768 Carter ME, Yizhar O, Chikahisa S, Nguyen H, Adamantidis A, Nishino S, Deisseroth K, De
769 Lecea L (2010) Tuning arousal with optogenetic modulation of locus coeruleus neurons.
770 Nat Neurosci 13:1526–1535.
771 Chauvette S, Seigneur J, Timofeev I (2012) Sleep Oscillations in the Thalamocortical System
772 Induce Long-Term Neuronal Plasticity. Neuron 75:1105–1113.
773 Cheng MY, Wang EH, Woodson WJ, Wang S, Sun G, Lee AG, Arac A, Fenno LE,
774 Deisseroth K, Steinberg GK (2014) Optogenetic neuronal stimulation promotes
775 functional recovery after stroke. Proc Natl Acad Sci 111:12913–12918.
776 Cook DJ, Teves L, Tymianski M (2012) Treatment of stroke with a PSD-95 inhibitor in the
777 gyrencephalic primate brain. Nature 483:213–217.
778 Csercsa R et al. (2010) Laminar analysis of slow wave activity in humans. Brain 133:2814–
779 2829.
780 Cui L, Murikinati SR, Wang D, Zhang X, Duan WM, Zhao LR (2013) Reestablishing
781 Neuronal Networks in the Aged Brain by Stem Cell Factor and Granulocyte-Colony
782 Stimulating Factor in a Mouse Model of Chronic Stroke. PLoS One 8:2–12.
783 Cummings BJ, Engesser-Cesar C, Cadena G, Anderson AJ (2007) Adaptation of a ladder
784 beam walking task to assess locomotor recovery in mice following spinal cord injury.
785 Behav Brain Res 177:232–241.

786 Doeppner TR, El Aanbouri M, Dietz GPH, Weise J, Schwarting S, Bähr M (2010)
787 Transplantation of TAT-Bcl-xL-transduced neural precursor cells: Long-term
788 neuroprotection after stroke. Neurobiol Dis 40:265–276.
789 Doyon J (2008) Motor sequence learning and movement disorders. Curr Opin Neurol
790 21:478–483.
791 Dromerick AW, Birkenmeier RL, Miller JP, Videen TO, Power WJ, Wolf SL, Edwards DF
792 (2009) Very Early Constraint-Induced Movement during Stroke Rehabilitation (
793 VECTORS). Neurology 73:195–201.
794 Duss SB, Seiler A, Schmidt MH, Pace M, Adamantidis A, Müri RM, Bassetti CL (2017) The
795 role of sleep in recovery following ischemic stroke: A review of human and animal data.
796 Neurobiol Sleep Circadian Rhythm 2:94–105.
797 Ebajemito JK, Furlan L, Nissen C, Sterr A (2016) Application of transcranial direct current
798 stimulation in neurorehabilitation: The modulatory effect of sleep. Front Neurol 7:54.
799 Etiévant A, Manta S, Latapy C, Magno LA V., Fecteau S, Beaulieu JM (2015) Repetitive
800 transcranial magnetic stimulation induces long-lasting changes in protein expression and
801 histone acetylation. Sci Rep 5:1–9.
802 Feigin VL, Norrving B, Mensah GA (2017) Global Burden of Stroke. Circ Res 120:439–448.
803 Fernández-Bouzas a, Harmony T, Fernández T, Aubert E, Ricardo-Garcell J, Valdés P, Bosch
804 J, Casián G, Sánchez-Conde R (2002) Sources of Abnorma EEG Activityin Spontaneous
805 Intracerebral Hemorrhage. Clin EEG Neurosci 33:70-76.
806 Funk CM, Peelman K, Bellesi M, Marshall W, Cirelli C, Tononi G (2017) Role of
807 Somatostatin-Positive Cortical Interneurons in the Generation of Sleep Slow Waves. J
808 Neurosci 37:9132–9148.
809 Gao B, Kilic E, Baumann CR, Hermann DM, Bassetti CL (2008) Gamma-hydroxybutyrate
810 accelerates functional recovery after focal cerebral ischemia. Cerebrovasc Dis 26:413–

419.

Gent TC, Bandarabadi M, Herrera CG, Adamantidis AR (2018) Thalamic dual control of sleep and wakefulness. Nat Neurosci 21:1–11.

Gerashchenko D, Wisor JP, Burns D, Reh RK, Shiromani PJ, Sakurai T, de la Iglesia HO, Kilduff TS (2008) Identification of a population of sleep-active cerebral cortex neurons. Proc Natl Acad Sci 105:10227–10232.

Giubilei F, Iannilli M, Vitale A, Pierallini A, Sacchetti ML, Antonini G, Fieschi C (1992) Sleep patterns in acute ischemic stroke. Acta Neurol Scand 86:567–571.

Grefkes C, Fink GR (2014) Connectivity-based approaches in stroke and recovery of function. Lancet Neurol 13:206–216.

Hermann DM, Siccoli M, Brugger P, Wachter K, Mathis J, Achermann P, Bassetti CL (2008) Evolution of Neurological, Neuropsychological and Sleep-Wake Disturbances After Paramedian Thalamic Stroke. Stroke 39:62–68.

Herrera CG, Cadavieco MC, Jego S, Ponomarenko A, Korotkova T, Adamantidis A (2016) Hypothalamic feedforward inhibition of thalamocortical network controls arousal and consciousness. Nat Neurosci 19:290–298.

Hodor A, Palchykova S, Baracchi F, Noain D, Bassetti CL (2014) Baclofen facilitates sleep, neuroplasticity, and recovery after stroke in rats. Ann Clin Transl Neurol 1:765–777.

Huang J, Upadhyay UM, Tamargo RJ (2006) Inflammation in stroke and focal cerebral ischemia. Surg Neurol 66:232–245.

Huber R, Ghilardi MF, Massimini M, Tononi G (2004) Local sleep and learning. Nature 430:78–81.

Irwin MR (2019) Sleep and inflammation: partners in sickness and in health. Nat Rev Immunol 19:702–715.

Irwin MR, Cole SW (2011) Reciprocal regulation of the neural and innate immune systems.

836 Nat Rev Immunol 11:625–632.
837 Jackson J, Ayzenshtat I, Karnani MM, Yuste R (2016) VIP+ interneurons control neocortical
838 activity across brain states. J Neurophysiol 115:3008–3017.
839 Jego S, Glasgow SD, Herrera CG, Ekstrand M, Reed SJ, Boyce R, Friedman J, Burdakov D,
840 Adamantidis AR (2013) Optogenetic identification of a rapid eye movement sleep
841 modulatory circuit in the hypothalamus. Nat Neurosci 16:1637–1643.
842 Kaneko Y, Floras JS, Usui K, Plante J, Tkacova R, Kubo T, Ando S, Bradley TD (2003)
843 Cardiovascular Effects of Continuous Positive Airway Pressure in Patients with Heart
844 Failure and Obstructive Sleep Apnea. N Engl J Med 348:1233–1241.
845 Khedr EM, Ahmed MA, Fathy N, Rothwell JC (2005) Therapeutic trial of repetitive
846 transcranial magnetic stimulation after acute ischemic stroke. Neurology 65:466–468.
847 Kielar A, Deschamps T, Chu RKO, Jokel R, Khatamian YB, Chen JJ, Meltzer JA (2016)
848 Identifying dysfunctional cortex: Dissociable effects of stroke and aging on resting state
849 dynamics in MEG and fmri. Front Aging Neurosci 8:40.
850 Kim YH, You SH, Ko MH, Park JW, Lee KH, Jang SH, Yoo WK, Hallett M (2006)
851 Repetitive transcranial magnetic stimulation-induced corticomotor excitability and
852 associated motor skill acquisition in chronic stroke. Stroke 37:1471–1476.
853 Lai TW, Zhang S, Wang YT (2014) Excitotoxicity and stroke: Identifying novel targets for
854 neuroprotection. Prog Neurobiol:157–188.
855 Landsness EC, Crupi D, Hulse BK, Peterson MJ, Huber R, Ansari H (2009) Sleep-Dependent
856 Improvement in Visuomotor Learning: A Causal Role for Slow Waves. Sleep 32:123–
857 184.
858 Liew S-L, Santarnecchi E, Buch ER, Cohen LG (2014) Non-invasive brain stimulation in
859 neurorehabilitation: local and distant effects for motor recovery. Front Hum Neurosci
860 8:378.

861 Lin TN, He YY, Wu G, Khan M, Hsu CY (1993) Effect of brain edema on infarct volume in
862 a focal cerebral ischemia model in rats. Stroke 24:117–121.
863 Lindenberg R, Renga V, Zhu LL, Nair D, Schlaug G (2010) Bihemispheric brain stimulation
864 facilitates motor recovery in chronic stroke patients. Neurology 75:2176–2184.
865 Liu Z, Li Y, Qu R, Shen L, Gao Q, Zhang X, Lu M, Savant-Bhonsale S, Borneman J, Chopp
866 M (2007) Axonal sprouting into the denervated spinal cord and synaptic and
867 postsynaptic protein expression in the spinal cord after transplantation of bone marrow
868 stromal cell in stroke rats. Brain Res 1149:172–180.
869 Liu Z, Zhang RL, Li Y, Cui Y, Chopp M (2009) Remodeling of the corticospinal innervation
870 and spontaneous behavioral recovery after ischemic stroke in adult mice. Stroke
871 40:2546–2551.
872 Lu Y, Jiang L, Qu M, Song Y, He X, Zhang Z, Yang G-Y, Wang Y (2017) Optogenetic
873 inhibition of striatal neurons improves the survival of implanted neural stem cell and
874 neurological outcomes after ischemic stroke in mice. Stem Cells Int 2017:11.
875 Massimini M, Huber R, Ferrarelli F, Hill S, Tononi G (2004) The Sleep Slow Oscillation as a
876 Traveling Wave. J Neurosci Res 24:6862-6870.
877 McCormick DA, McGinley MJ, Salkoff DB (2015) Brain state dependent activity in the
878 cortex and thalamus. Curr Opin Neurobiol 31:133–140.
879 Mensen A, Riedner B, Tononi G (2016) Optimizing detection and analysis of slow waves in
880 sleep EEG. J Neurosci Methods 274:1–12.
881 Miyamoto D, Jirai D, Fung CCA, Inutsuka A, Odagawa M, Suzuki T, Boehringer R,
882 Adaikkan C, Matsubara C, Matsuki N, Fukai T, McHugh TJ, Yamanaka A, Murayama
883 (2016) Top-down cortical input during NREM sleep consolidates perceptual memory.
884 Science 352:1315-1318.
885 Murphy TH, Corbett D (2009) Plasticity during stroke recovery: from synapse to behaviour.

886 Nat Rev Neurosci 10:861–872.
887 Murri L, Gori S, Massetani R, Bonanni E, Marcella F, Milani S (1998) Evaluation of acute
888 ischemic stroke using quantitative EEG: A comparison with conventional EEG and CT
889 scan. Neurophysiol Clin 28:249-257.
890 Ng K, Gibson EM, Hubbard R, Yang J, Caffo B, O'Brien R, Krakauer JW, Zeiler SR (2015)
891 Fluoxetine maintains a state of heightened responsiveness to motor training early after
892 stroke in a mouse model Kwan. Stroke 46:2951–2960.
893 Ngo HV V., Claussen JC, Born J, Mölle M (2013) Induction of slow oscillations by rhythmic
894 acoustic stimulation. J Sleep Res 22:22–31.
895 Niethard N, Hasegawa M, Itokazu T, Oyanedel CN, Born J, Sato TR (2016) Sleep-Stage-
896 Specific Regulation of Cortical Excitation and Inhibition. Curr Biol 26:2739–2749.
897 Niimi M, Sasaki N, Kimura C, Hara T, Yamada N, Abo M (2018) Sleep during low-
898 frequency repetitive transcranial magnetic stimulation is associated with functional
899 improvement in upper limb hemiparesis after stroke. Acta Neurol Belg 119:1–6.
900 Nudo RJ (1997) Remodeling of cortical motor representations after stroke: implications for
901 recovery from brain damage. Mol Psychiatry 2:188–191.
902 Nudo RJ (2006) Mechanisms for recovery of motor function following cortical damage. Curr
903 Opin Neurobiol 16:638–644.
904 Panagiotou M, Vyazovskiy V V., Meijer JH, Deboer T, Czeisler CA (2017) Differences in
905 electroencephalographic non-rapid-eye movement sleep slow-wave characteristics
906 between young and old mice. Sci Rep 7:43656.
907 Park SY, Marasini S, Kim GH, Ku T, Choi C, Park MY, Kim EH, Lee YD, Suh-kim H, Kim
908 SS (2014) A method for generate a mouse model of stroke: evaluation of parameters for
909 blood flow, behavior, and survival. Exp Neurobiol 23:104–114.
910 Poryazova R, Huber R, Khatami R, Werth E, Brugger P, Barath K, Baumann CR, Bassetti CL

(2015) Topographic sleep EEG changes in the acute and chronic stage of hemispheric stroke. J Sleep Res 24:54-65.

Puentes-Mestril C, Aton SJ (2017) Linking Network Activity to Synaptic Plasticity during Sleep: Hypotheses and Recent Data. Front Neural Circuits 11:1–18.

Robinson RG, Jorge RE, Moser DJ, Acion L, Solodkin A, Small SL, Fonzetti P, Hegel M, Arndt S (2008) Escitalopram and problem-solving therapy for prevention of poststroke depression: A randomized controlled trial. JAMA - J Am Med Assoc 299:2391–2400.

Rodriguez A V, Funk CM, Vyazovskiy V V, Nir Y, Tononi G, Cirelli C (2016) Why Does Sleep Slow-Wave Activity Increase After Extended Wake? Assessing the Effects of Increased Cortical Firing During Wake and Sleep. J Neurosci 36:12436–12447.

Rosanova M, Ulrich (2005) Pattern-Specific Associative Long-Term Potentiation Induced by a Sleep Spindle-Related Spike Train. J Neurosci 25:9398–9405.

Sarasso S, Määttä S, Ferrarelli F, Poryazova R, Tononi G, Small SL (2014) Plastic Changes Following Imitation-Based Speech and Language Therapy for Aphasia. Neurorehabil Neural Repair 28:129–138.

Shah AM, Ishizaka S, Cheng MY, Wang EH, Bautista AR, Levy S, Smerin D, Sun G, Steinberg GK (2017) Optogenetic neuronal stimulation of the lateral cerebellar nucleus promotes persistent functional recovery after stroke. Sci Rep 7:46612.

Siccoli MM, Rölli-Baumeler N, Achermann P, Bassetti CL (2008) Correlation between sleep and cognitive functions after hemispheric ischaemic stroke. Eur J Neurol 15:565–572.

Silasi G, Murphy TH (2014) Stroke and the Connectome: How Connectivity Guides Therapeutic Intervention. Neuron 83: 1354-1368.

Small DL, Morley P, Buchan AM (1999) Biology of ischemic cerebral cell death. Prog Cardiovasc Dis 42:185–207.

Steriade M, Nuñez A, Amzica F (1993) A novel slow(<1 Hz) oscillation of

936 neocorticalneurons in vivo: depolarizing and hyperpolarizing components. J Neurosci
937 13:3252–3265.
938 Steriade M, Timofeev I, Grenier F (2001) Natural waking and sleep states: a view from inside
939 neocortical neurons. J Neurophysiol 85:1969–1985.
940 Stroh A, Adelsberger H, Groh A, Rühlmann C, Fischer S, Schierloh A, Deisseroth K,
941 Konnerth A (2013) Making Waves: Initiation and Propagation of Corticothalamic Ca2+
942 Waves In Vivo. Neuron 77:1136–1150.
943 Sun Y, Cheng X, Wang H, Mu X, Liang Y, Luo YJ, Qu H, Zhao C (2017) DL-3-n-
944 butylphthalide promotes neuroplasticity and motor recovery in stroke rats. Behav Brain
945 Res 329:67–74.
946 Talelli P, Wallace A, Dileone M, Hoad D, Cheeran B, Oliver R, VandenBos M, Hammerbeck
947 U, Barratt K, Gillini C, Musumeci G, Boudrias M-H, Cloud GC, Ball J, Marsden JF,
948 Ward NS, Di Lazzaro V, Greenwood RG, Rothwell JC (2012) Theta Burst Stimulation
949 in the Rehabilitation of the Upper Limb. Neurorehabil Neural Repair 26:976–987.
950 Tennant KA, Taylor SL, White ER, Brown CE (2017) Optogenetic rewiring of
951 thalamocortical circuits to restore function in the stroke injured brain. Nat Commun
952 8:15879.
953 Timofeev I, Chauvette S (2017) Sleep slow oscillation and plasticity. Curr Opin Neurobiol
954 44:116–126.
955 Tononi G, Cirelli C (2006) Sleep function and synaptic homeostasis. Sleep Med Rev 10:49–
956 62.
957 Tononi G, Cirelli C (2014) Neuron Perspective Sleep and the Price of Plasticity: From
958 Synaptic and Cellular Homeostasis to Memory Consolidation and Integration. Neuron
959 81:12–34.
960 Tononi G, Cirelli C (2016) Sleep and Synaptic Down-Selection. In: European Journal of

961 Neuroscience, pp 99–106.
962 van Meer MPA, Otte WM, van der Marel K, Nijboer CH, Kavelaars A, van der Sprenkel
963 JWB, Viergever MA, Dijkhuizen RM (2012) Extent of Bilateral Neuronal Network
964 Reorganization and Functional Recovery in Relation to Stroke Severity. J Neurosci
965 32:4495–4507.
966 Vock J, Achermann P, Bischof M, Milanova M, Müller C, Nirkko A, Roth C, Bassetti CL
967 (2002) Evolution of sleep and sleep EEG after hemispheric stroke. J Sleep Res 11:331–
968 338.
969 Vyazovskiy V V, Faraguna U, Cirelli C, Tononi G (2009) Triggering slow waves during
970 NREM sleep in the rat by intracortical electrical stimulation: effects of sleep/wake
971 history and background activity. J Neurophysiol 101:1921–1931.
972 Vyazovskiy V V., Olcese U, Hanlon EC, Nir Y, Cirelli C, Tononi G (2011) Local sleep in
973 awake rats. Nature 472:443–447.
974 Vyazovskiy V V., Olcese U, Lazimy YM, Faraguna U, Esser SK, Williams JC, Cirelli C,
975 Tononi G (2009) Cortical Firing and Sleep Homeostasis. Neuron 63:865–878.
976 Xie L, Kang H, Xu Q, Chen MJ, Liao Y, Thiyagarajan M, O'Donnell J, Christensen DJ,
977 Nicholson C, Iliff JJ, Takano T, Deane R, Nedergaard M (2013) Sleep drives metabolite
978 clearance from the adult brain. Science (80-) 342:373–377.
979 Yang G, Lai C, Cichon J, Ma L, Li W, Gan W-B (2014) Sleep promotes branch-specific
980 formation of dendritic spines after learning. Science (80-) 344:1173–1178.
981 Yokoyama E, Nagata K, Hirata Y, Satoh Y, Watahiki Y, Yuya H (1996) Correlation of EEG
982 activities between slow-wave sleep and wakefulness in patients with supra-tentorial
983 stroke. Brain Topogr 8:269-273.
984 Yoon KJ, Oh B-M, Kim D-Y (2012) Functional improvement and neuroplastic effects of
985 anodal transcranial direct current stimulation (tDCS) delivered 1day vs. 1week after

cerebral ischemia in rats. Brain Res 1452:61–72.

Xu W, De Carvalho F, Jackson A (2019) Sequential neural activity in primary motor cortex during sleep. J Neurosci 39:3698–3712.

Zhang X, Mei Y, Liu C, Yu S (2007) Effect of transcranial magnetic stimulation on the expression of c-Fos and brain-derived neurotrophic factor of the cerebral cortex in rats with cerebral infarct. J Huazhong Univ Sci Technol 27:415–418.

Zucca S, D'Urso G, Pasquale V, Vecchia D, Pica G, Bovetti S, Moretti C, Varani S, Molano-Mazón M, Chiappalone M, Panzeri S, Fellin T (2017) An inhibitory gate for state transition in cortex. Elife 6:1–31.

FIGURE LEGENDS

Figure 1. Stroke alters sleep architecture. (A) Schematic of the Circle of Willis (CW) with highlighted common carotid artery (CCA), internal carotid artery (ICA), middle cerebral artery (MCA) involved in MCAo procedure and filament placement. (B) Coronal sections (40 µm) of a representative mouse 15 days after MCAo. Nissl staining. (C) Schematic representation of EEG and EMG electrodes placements relative to stroke. 24 h recordings of animals' sleep-wake cycles were performed before stroke (Baseline) and again at post-stroke day 1, 3, 5 and 10 in Stroke (n = 11) and Sham (n = 9) animals. (D) Percentage changes of wakefulness, NREM sleep (E) and REM sleep (F) total durations from each animal's baseline values. (G) Comparison between bout durations of wakefulness, NREM sleep (H) and REM sleep (I). (J) Ratio between NREM continuous episodes and transitions to wake. (K) Total number of microarousals in 24 h recordings. (L) Percentage of epochs spent in wake or sleep states for Stroke (blue table) and Sham (grey table) groups, respectively. Linear mixed model of 8 matrices: Wake duration changes; NREM duration changes; REM duration changes; Wake bout duration; NREM bout duration; REM bout duration; NREM stability; Microarousals. Data are represented as means ± s.e.m.; asterisks indicate significance *$p < 0.0063$.

Figure 2. Stroke alters SW profile. (A) Automatic detection of single slow waves (SW) from local field potential (LFP) recordings in ipsilateral primary somatosensory forelimb cortex (iS1FL), ipsilateral primary motor cortex (iM1), contralateral M1 (cM1), contralateral S1FL (cS1FL) and EEG traces from ipsilateral (iEEG) and contralateral (cEEG) hemispheres. Representative traces in black and detected SW in colours (top). Magnification of one episode of NREM sleep and detected SW (bottom). (B) Schematic of tetrodes and EEG/EMG electrode implantation. (C) Representative average SW from 24 h baseline EEG recording.

(D) Unit activity heat map of neurons recorded during detected SW; the graph shows neuronal activity suppression corresponding to the silent SW DOWN state (top). Average firing rate of single units recorded during the detected SW (bottom). (E) Schematic of EEG electrodes position. (F) SW peak to peak amplitude prior to (Baseline) and following MCAo or sham surgery (post stroke day 1, 3, 5 and 10). (G) SW positive slope. (H) SW negative slope. (I) Number of single SW detected. (J) SW duration. Stroke n = 11, Sham n = 9; two-way ANOVA, followed by Bonferroni post-hoc test. Data are represented as means ± s.e.m. Asterisks indicate significance *$p < 0.05$.

Figure 3. Optogenetic induction of SW-like bistable oscillations. (A) Scheme of a coronal brain section with AAV injection site (left), AAV structure (top) and optrode/EEG/EMG implantation representation (right). (B) Opsin distribution within the peri-infarct ipsilateral primary somatosensory forelimb cortex (iS1FL) following AAV injection of CaMKII-ChR2-EYFP. (C) Local field potential (LFP) traces, single unit activity and correspondent raster plot and mean spike rate upon optogenetic stimulation during wakefulness (left), NREM sleep (middle) and REM sleep (right) from one representative stimulation session. (D) Average ipsilateral (iEEG) and contralateral EEG (cEEG) traces response to activation (ChR2) of pyramidal neurons with 5 ms of single laser light pulses (473 nm). (E) Comparison between spontaneous and optogenetically-evoked SW (SW^{opto}) duration (left), negative amplitude (middle) and slope (right) during NREM sleep for ChR2 stimulated animals; Wilcoxon rank sum test, statistically significant if $p < 0.05$. (F) ArchT distribution within iS1FL. (G) Representative EEG/EMG traces upon silencing of pyramidal neurons with 200 ms of single laser light pulses (532 nm) during NREM sleep. (H) Average iEEG and cEEG responses to ArchT stimulation. (I) Comparison between SW^{opto} duration (left), negative amplitude (middle) and slope (right) during NREM sleep for ArchT stimulated animals;

1047 Wilcoxon rank sum test, statistically significant if $p < 0.05$. (J) mCherry (control) expression
1048 in iS1FL; representative EEG/EMG responses during 5ms light pulse stimulation (top) and
1049 average EEGs (bottom). (L) Representative EEG/EMG traces response to 200ms pulse
1050 stimulation in one mCherry transfected mouse (top) and its average EEGs response.
1051
1052 **Figure 4.** Optogenetic screening for slow waves induction in the peri-infarct zone. (A)
1053 Coronal section indicating the AAV injection site (left primary somatosensory forelimb
1054 cortex, S1FL) (top) and schematic of EEG/EMG/optic fiber/tetrodes implantation (bottom).
1055 (B) LFP recordings from S1FL upon laser light stimulation (500 ms, 5 Hz and 200 ms) of
1056 inhibitory (top) or pyramidal neurons (bottom) respectively.
1057
1058 **Figure 5.** SW^{opto} oscillations travel across hemispheres. (A) Local field potential (LFP)
1059 traces, multi-unit activity from tetrodes placed in ipsilateral primary somatosensory forelimb
1060 cortex (iS1FL), contralateral S1FL (cS1FL), ipsilateral primary motor cortex (iM1) and
1061 contralateral M1 (cM1) and EEG/EMG traces recorded during one stimulating session
1062 showing the travelling characteristic of the evoked waves (SW^{opto}). (B) Raster plots
1063 corresponding to one single light pulse stimulation event during wakefulness, NREM and
1064 REM sleep as well as relative mean spike rate for iS1FL, cS1FL, cM1 respectively. No unit
1065 was found for iM1. (C) Average LFP traces during the stimulation events for the four
1066 recorded cortical areas respectively.
1067
1068 **Figure 6.** SW^{opto} defines a critical window of intervention for stroke recovery. (A) When the
1069 stimulation protocol started at post-stroke day 1, $ChR2^{stroke}$ animals in particular showed
1070 lower survival percentage. (B) When the stimulation instead began at post-stroke day 5,

1071 $ChR2^{stroke}$ animal showed an improvement in survival percentage. Asterisks indicate
1072 significance *$p < 0.05$.
1073
1074 **Figure 7.** SW^{opto} during sleep improves functional recovery after stroke. (A) Schematics of
1075 optic fiber/EEG/EMG implantation with opsin expression site. (B) Experimental timeline. (C)
1076 Average number of single light pulses within sleep stages during the stimulation sessions of
1077 $ArchT^{stroke}$, $ChR2^{stroke}$, $mCherry^{stroke}$, $mCherry^{sham}$ and $ChR2^{stroke\_wake}$ respectively. (D)
1078 Stimulated animals showed better performances in the ladder walking rig test compared to
1079 mCherry-control animals (Naive n = 8, $mCherry^{sham}$ n = 8, $ArchT^{stroke}$ n = 4, $ChR2^{stroke}$ n = 7,
1080 $mCherry^{stroke}$ n = 6). Induction of slow waves mainly during wakefulness ($ChR2^{stroke\_wake}$ n =
1081 6) did not result in faster improvement of performance compared to $ChR2^{stroke}$ stimulated
1082 during NREM sleep. Linear mixed model. (E) Percentage of improvement from post-stroke
1083 day 4 to post-stroke day 15 for $ChR2^{stroke}$ groups and $ArchT^{stroke}$ compared to $mCherry^{stroke}$
1084 control (one-way ANOVA). (F) Similar results was observed for performances in the balance
1085 test (Naive n = 8, $mCherry^{sham}$ n = 6, $ArchT^{stroke}$ n = 7, $ChR2^{stroke}$ n = 7, $mCherry^{stroke}$ n = 7,
1086 $ChR2^{stroke\_wake}$ n = 6). (G) Balance beam percentage of improvement from post-stroke day 4
1087 to post-stroke day 15 for $ChR2^{stroke}$ groups and $ArchT^{stroke}$ compared to $mCherry^{stroke}$ control
1088 (one-way ANOVA). (H) Tight rope test and corner test (I) did not show differences between
1089 stimulated and control groups (Naive n = 8, $mCherry^{sham}$ n = 6, $ArchT^{stroke}$ n = 7, $ChR2^{stroke}$ n
1090 = 6, $mCherry^{stroke}$ n = 8, $ChR2^{stroke\_wake}$ n = 6). Asterisks indicate significances *$p < 0.05$.
1091
1092 **Figure 8.** SW^{opto} increases axonal sprouting during stroke recovery. (A) Scheme of a brain
1093 coronal section 15 days after stroke (end point of experiment) representing tissue atrophy
1094 corresponding to the stroke area. Confocal micrography of iS1FL with 3D reconstruction of
1095 pre- and post-synaptic markers contact (right). Blue: DAPI staining; red: Vglut1 pre-synaptic

marker; acquamarine: PSD-95 post-synaptic marker. (B) Comparison of Vglut1 puncta density between iS1FL and cS1FL cortical areas ($mCherry^{stroke}$ n = 4, $ChR2^{stroke}$ n = 4, $ArchT^{stroke}$ n = 4, $mCherry^{sham}$ n = 4) in ipsilateral ($F_{(3, 19)} = 10.49$, $p = 0.0003$) and contralateral layers II ($F_{(3, 19)} = 1.069$, $p = 0.385$), as well as in ipsilateral ($F_{(3, 18)} = 16.02$, $p < 0.0001$) and contralateral layers V ($F_{(3, 21)} = 11.05$, $p = 0.0001$) (C). (D) Vglut1 puncta volume distribution in iS1FL layer II ($F_{(2, 1630)} = 34.85$, $p < 0.0001$) and layer V (E) summarized in bar graph ($F_{(2, 1617)} = 155$, $p < 0.0001$). (F) Comparison of PSD-95 puncta density in ipsilateral ($F_{(3, 23)} = 8.609$, $p = 0.0005$) and contralateral ($F_{(3, 21)} = 1.105$, $p = 0.369$) layers II, as well as in ipsilateral ($F_{(3, 24)} = 1.095$, $p = 0.370$) and contralateral ($F_{(3, 24)} = 2.498$, $p = 0.083$) layers V (G). (H) PSD-95 puncta volume distribution in iS1FL layer II summarized in bar graph ($F_{(2, 2070)} = 9.164$, $p = 0.0001$); (I) iS1FL layer V ($F_{(2, 2111)} = 75.13$, $p < 0.0001$). One way-ANOVA. Data are represented as means ± s.e.m. Asterisks indicate significance *$p < 0.05$. n.s. = not significant.

Figure 1

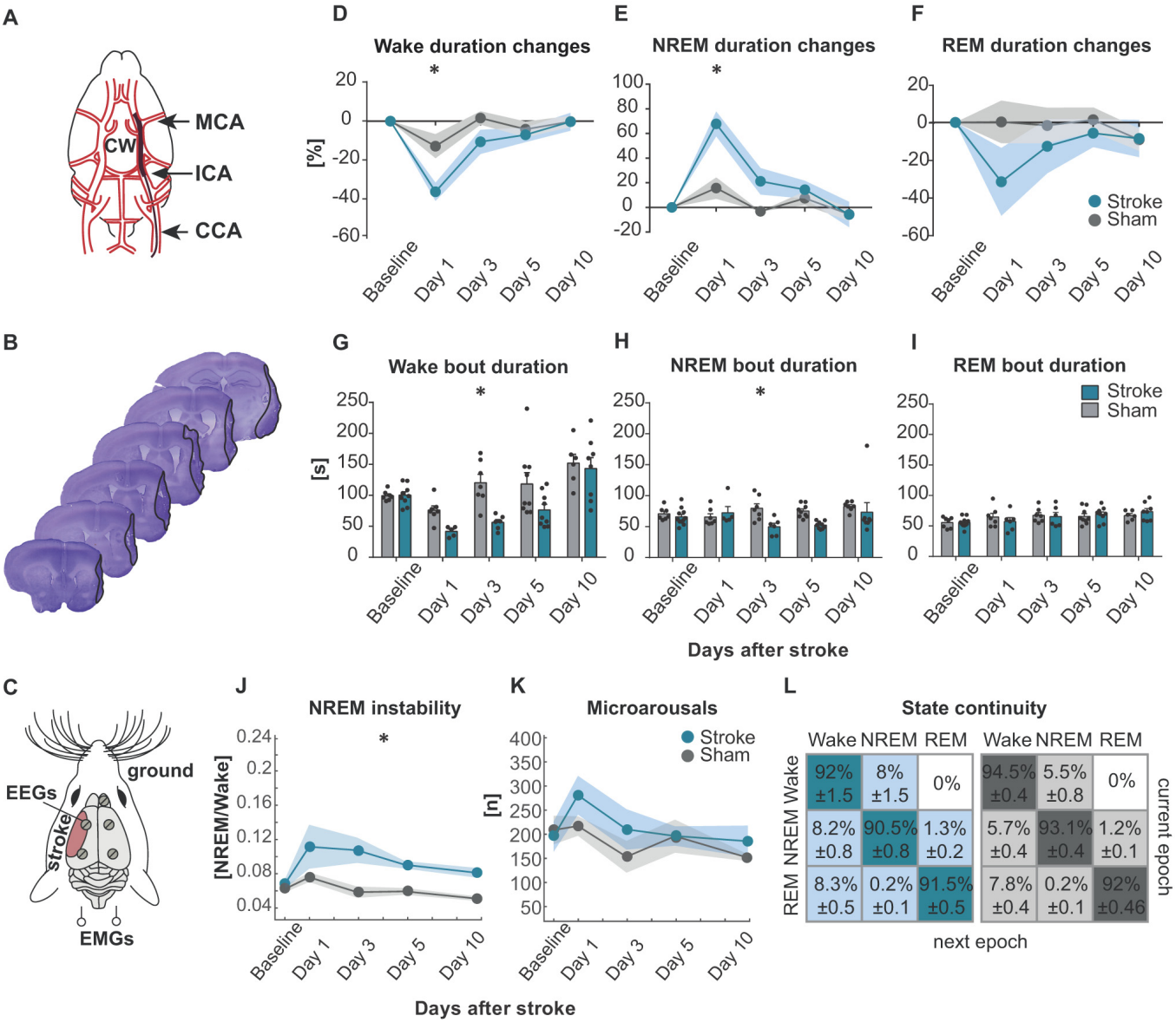

Figure 2

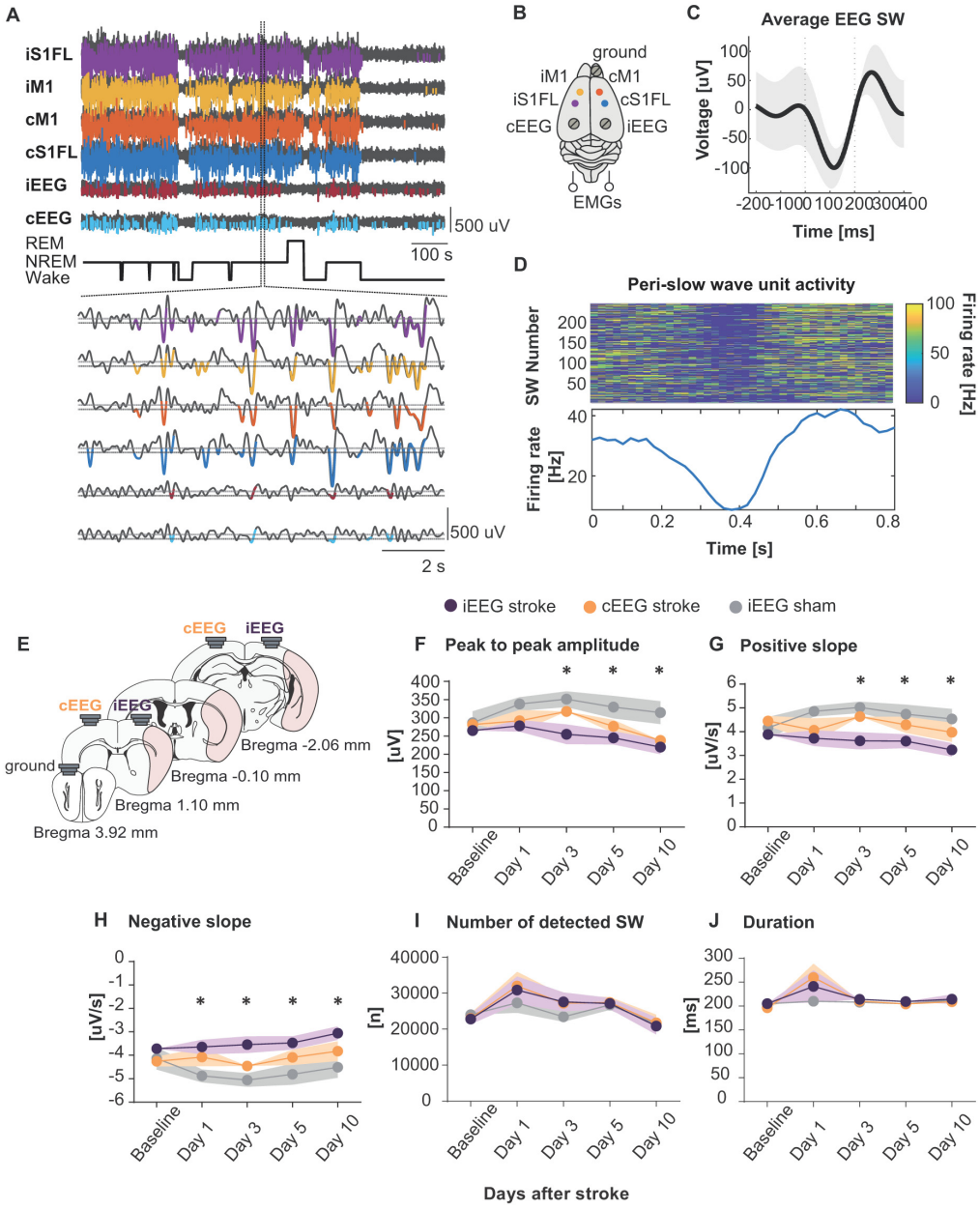

Figure 3

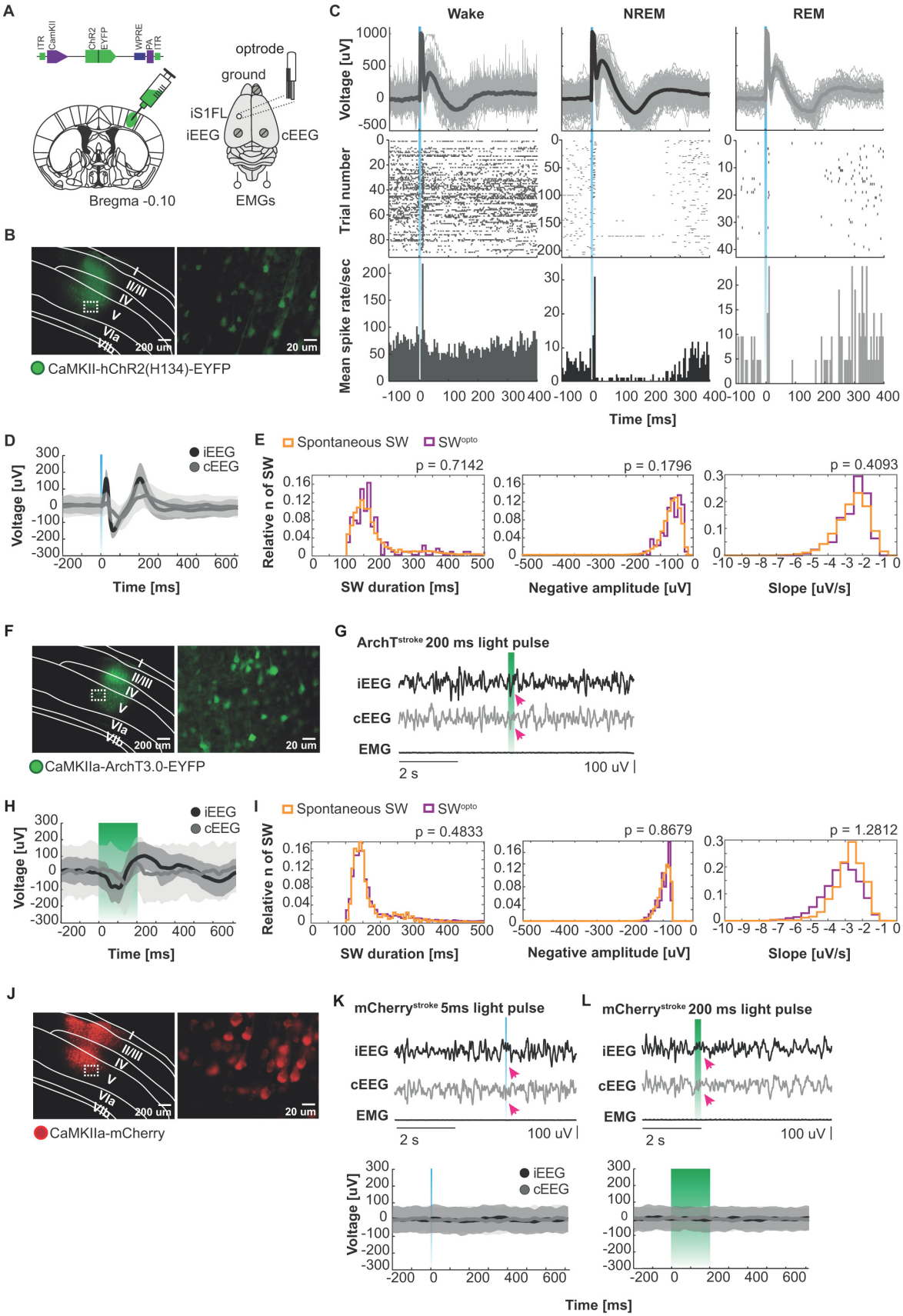

Figure 4

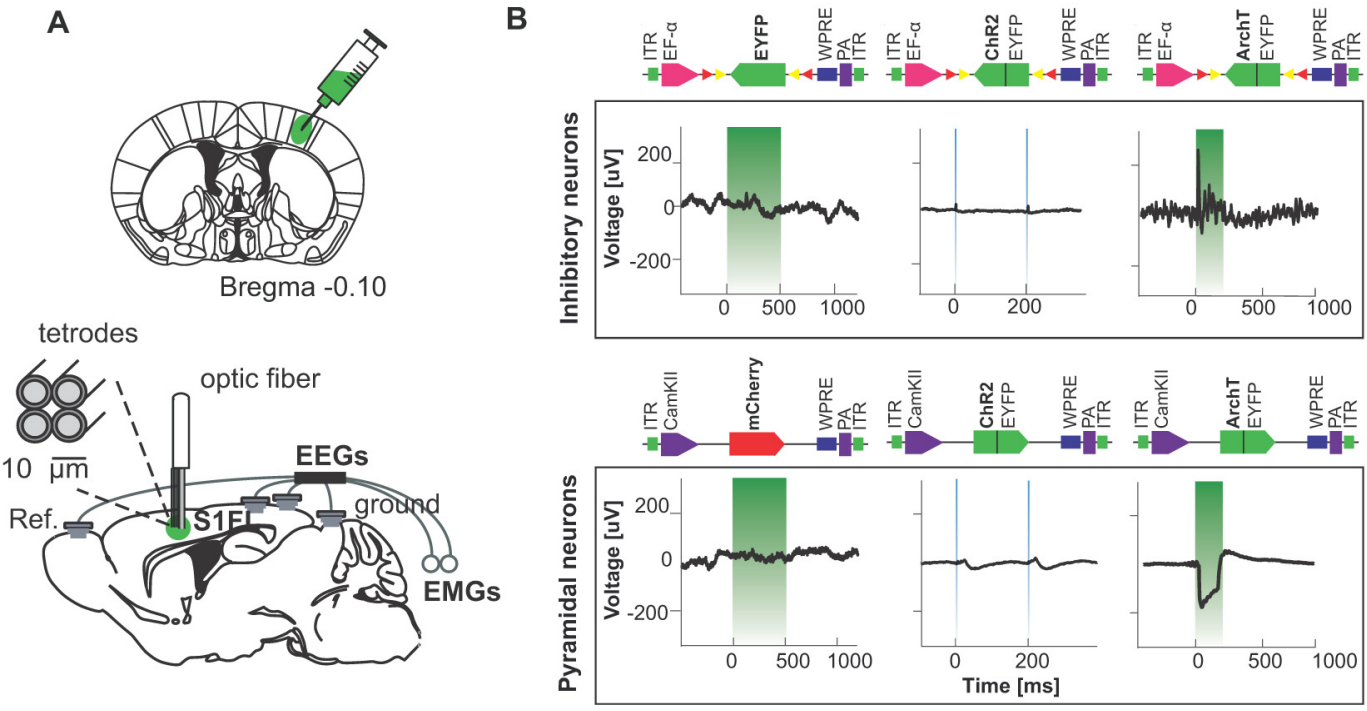

Figure 5

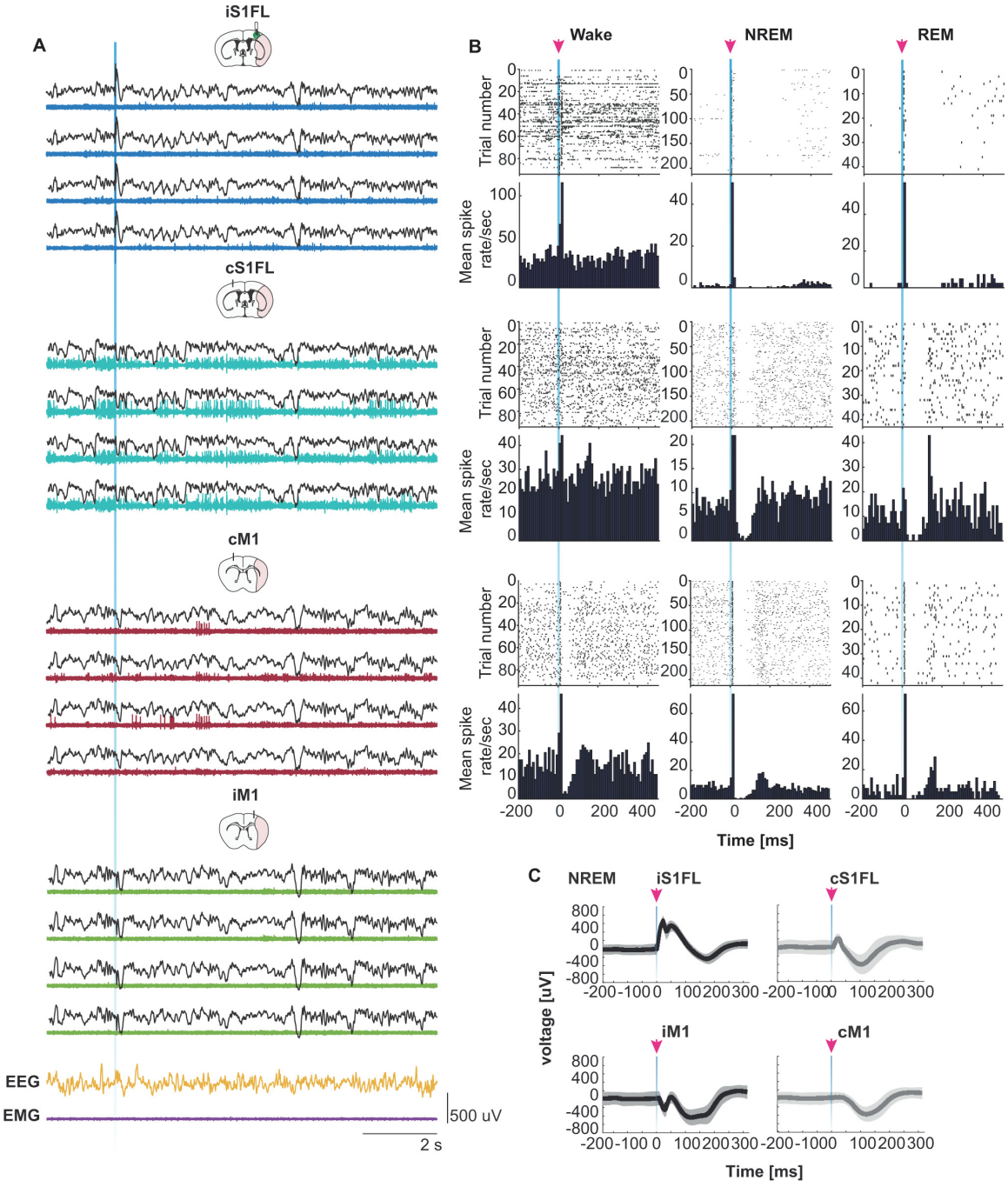

Figure 6

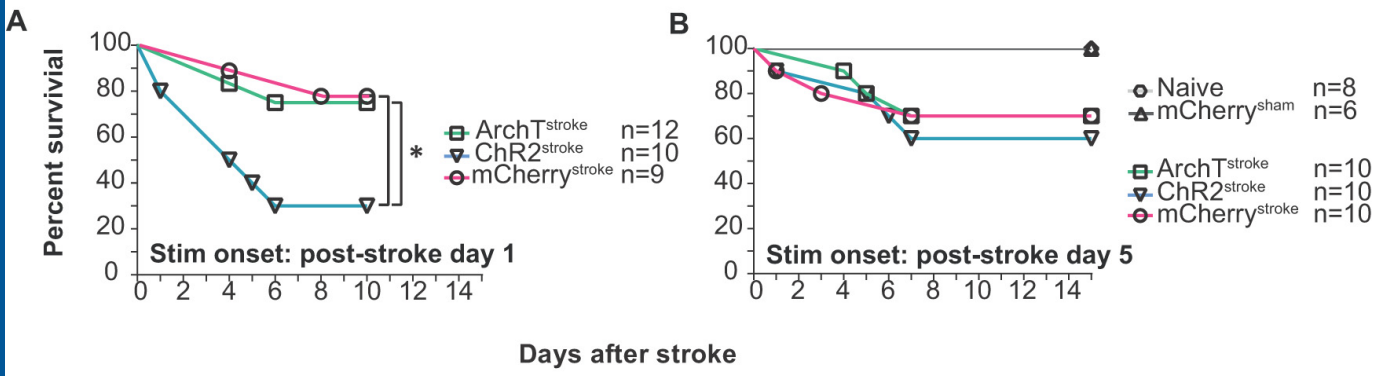

Figure 7

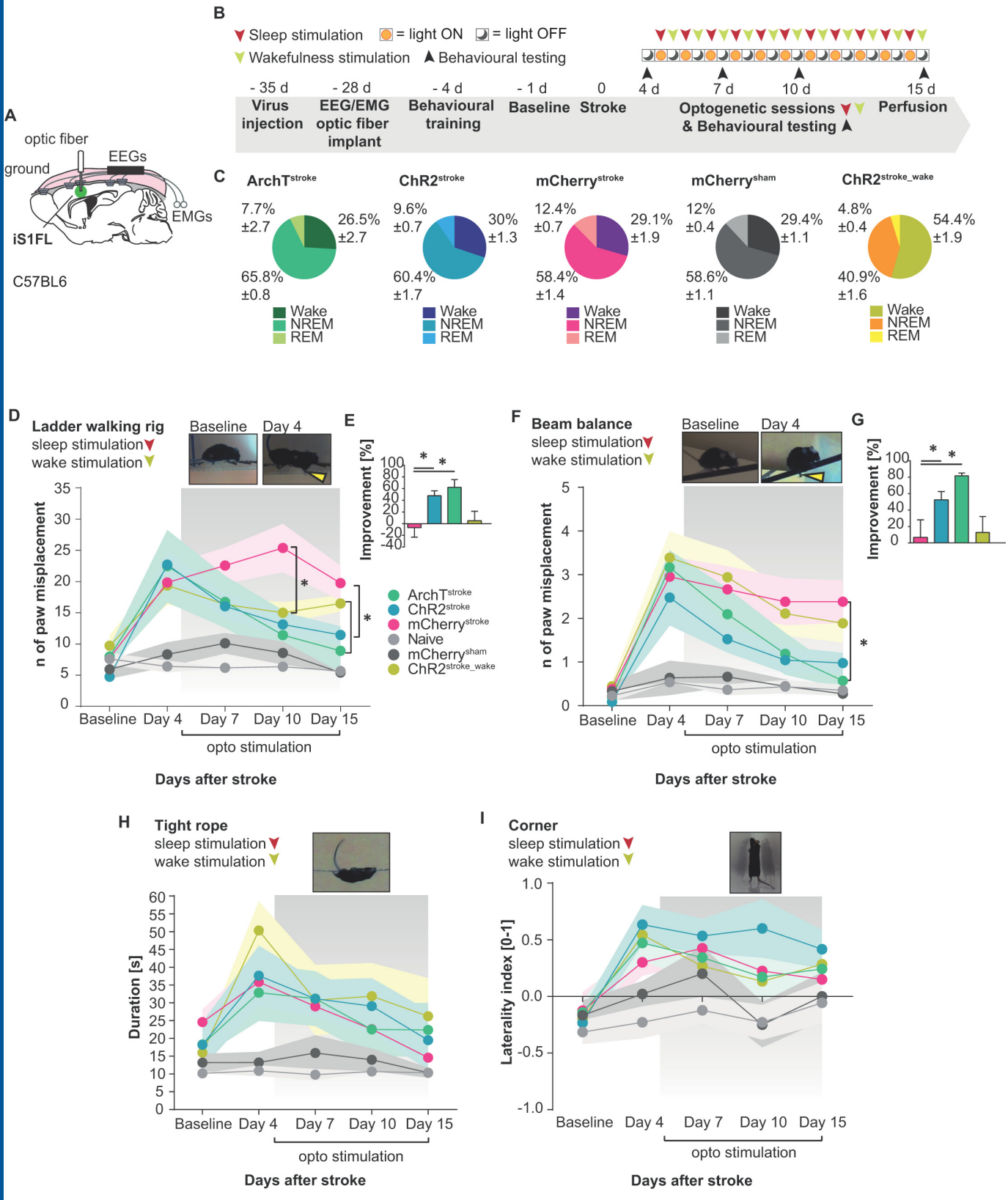

Figure 8